Dendrimer Ligand Directed Nanoplate Assembly

Katherine C. Elbert,[†,#] Thi Vo,[‡,#] Nadia M. Krook,[§] William Zygmunt,[‡] Jungmi Park,[†] Kevin G. Yager,[‖] Russell J. Composto,[§] Sharon C. Glotzer,[*,‡,⊥,¶] Christopher B. Murray[*,†,§]

[†] Department of Chemistry, University of Pennsylvania, Philadelphia, PA 19104, United States
[‡] Department of Chemical Engineering, University of Michigan, Ann Arbor, MI, 48109, United States
[§] Department of Materials Science and Engineering, University of Pennsylvania, Philadelphia, PA 19104, United States
[‖] Center for Functional Nanomaterials, Brookhaven National Laboratory, Upton, New York, 11973, United States
[⊥] Department of Materials Science and Engineering, University of Michigan, Ann Arbor, MI, 48109, United States
[¶] Biointerfaces Institute, University of Michigan, Ann Arbor, MI, 48109, United States

Table of Contents

Synthesis of Dendritic Ligands

Scheme S1. Synthesis of generation 2 dendrimer ligands.

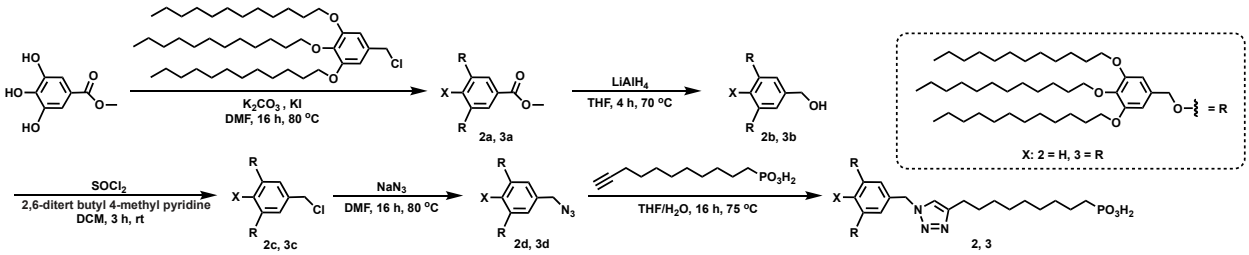

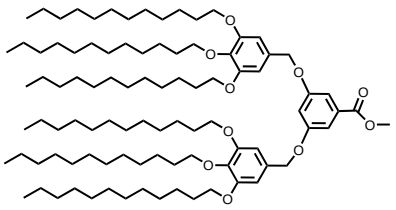

Methyl 3,5-bis((3,4,5-tris(dodecyloxy)benzyl)oxy)benzoate, 2a. Was synthesized as reported previously.[1] To a reaction flask was added 5-(chloromethyl)-1,2,3-tris(dodecyloxy)benzene (9.34 g, 13.74 mmol), methyl 3,5 dihydroxybenzoate (0.66 g, 3.92 mmol), K_2CO_3 (2.17 g, 15.70 mmol), KI (0.20 g, cat), and DMF (100 mL). The reaction mixture was heated to 80 °C for 20 hours and was subsequently cool to room temperature, diluted with $CHCl_3$ (150 mL), washed with H_2O (2 x 50 mL)), and 1 M HCl (2 x 50 mL). The resulting organic layers were dried with Na_2SO_4, filtered, and concentrated under vacuum. The crude product was purified with column chromatography (hexanes → hexanes:EtOAc 100:5), to afford pure **2a** as a white solid (4.33 g, 76 %). ^{1}H NMR ($CDCl_3$) δ 7.31 (d, J = 2.3 Hz, 2H), 6.81 (t, J = 2.4 Hz, 1H), 6.63 (s, 4H), 4.96 (s, 4H), 3.99 (q, J = 6.6 Hz, 12H), 3.91 (s, 3H), 1.84 – 1.75 (m, 12H), 1.50 (q, J = 7.6, 7.1 Hz, 12H), 1.36 – 1.26 (m, 96H), 0.92 – 0.87 (m, 18H); ^{13}C NMR ($CDCl_3$) δ 166.83, 159.96, 153.50, 138.29, 132.16, 131.49, 108.55, 107.39, 106.41, 73.56, 70.85, 69.30, 52.32, 32.14, 32.12, 30.55, 29.95, 29.93, 29.90, 29.85, 29.83, 29.81, 29.62, 29.59, 29.56, 26.34, 26.31, 22.87, 14.26; MALDI-TOF (m/z): $[M+Na]^+$ calcd. for $C_{94}H_{164}O_{10}Na$, 1476.22; found 1479.089.

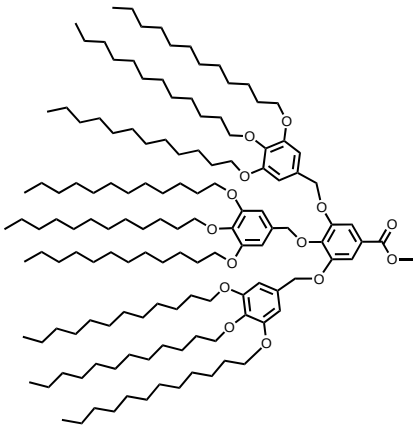

Methyl 3,4,5-tris((3,4,5-tris(dodecyloxy)benzyl)oxy)benzoate, 3a. As for **2a**. Methyl 3,4,5 trihydroxybenzoate (0.33 g, 1.81 mmol), 5-(chloromethyl)-1,2,3-tris(dodecyloxy)benzene (4.00 g, 5.89 mmol), K_2CO_3 (1.0 g, 7.25 mmol), KI (cat), 50 mL DMF. **3a** was isolated as an off-white solid (2.79 g, 73 %). ^{1}H NMR ($CDCl_3$) δ 7.38 (s, 2H), 6.63 (s, 4H), 6.60 (s, 2H), 5.04 (d, J = 5.1 Hz, 6H), 3.93 (t, J = 6.6 Hz, 4H), 3.91 – 3.86 (m, 14H), 3.76 (t, J = 6.4 Hz, 3H), 1.77 – 1.69 (m, 18H), 1.49 – 1.40 (m, 18H), 1.32 – 1.26 (m, 144H), 0.88 (t, J = 6.7 Hz, 27H); ^{13}C NMR ($CDCl_3$) δ 166.72, 153.50, 153.24, 152.79, 142.78, 138.13, 138.08, 132.60, 131.88, 125.46, 109.88, 106.51, 105.98, 75.37, 73.61, 73.53, 71.91, 69.32, 69.14, 52.38, 32.18, 32.17, 30.66, 30.64, 30.05, 30.01, 30.00, 29.97, 29.94, 29.92, 29.90, 29.86, 29.81, 29.73, 29.69, 29.64, 29.62, 26.45, 26.41, 26.40, 22.92, 14.33; MALDI-TOF (m/z): $[M+Na]^+$ calcd. for $C_{137}H_{242}O_{14}Na$, 2134.82; found 2140.689.

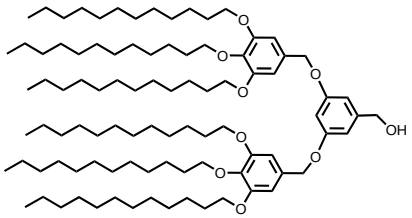

(3,5-Bis((3,4,5-tris(dodecyloxy)benzyl)oxy)phenyl)methanol, 2b. In a reaction flask was combined $LiAlH_4$ (0.60 g, 15.84 mmol) and THF (100 mL) at 0 °C, followed by slow addition of **2a** (5.75 g, 3.96 mmol). The reaction mixture was then heated to 70 °C for 4 hours. Then the reaction mixture was cooled to 0 °C before being quenched slowly with ice water. The solution was then concentrated under reduced pressure, dissolved in $CHCl_3$ (100 mL), and washed with 1 M HCl (2 x 50 mL), followed by being dried with Na_2SO_4, filtered, and concentrated under pressure. **2b** was isolated as a white solid (4.74 g, 84 %). ^{1}H NMR ($CDCl_3$) δ 6.63 – 6.60 (m, 6H), 6.54 (t, J = 2.4 Hz, 1H), 4.90 (s, 4H), 4.62 (s, 2H), 3.97 (q, J = 6.3 Hz, 12H), 1.82 – 1.73 (m, 12H), 1.51 – 1.45 (m, 12H), 1.34 – 1.27 (m, 96H), 0.91 – 0.88 (m, 18H); ^{13}C NMR ($CDCl_3$) δ 160.30, 153.45, 143.77, 138.15, 131.91, 106.37, 105.79, 101.37, 77.43, 73.58, 70.62, 69.30, 65.27, 32.12, 32.11, 30.53, 29.94, 29.92, 29.89, 29.88, 29.84, 29.83, 29.81, 29.62, 29.57, 29.55, 26.33, 26.31, 22.86, 14.26; MALDI-TOF (m/z): $[M+Na]^+$ calcd. for $C_{93}H_{164}O_9Na$, 1448.23; found 1451.045.

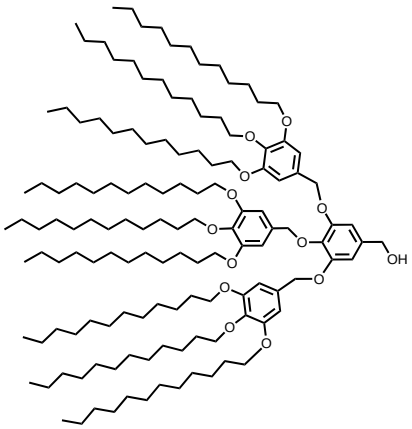

(3,4,5-Tris((3,4,5-tris(dodecyloxy)benzyl)oxy)phenyl)methanol, 3b. As for **2b**. **3a** (1.00 g, 0.48 mmol), $LiAlH_4$ (0.06 g, 1.45 mmol), THF (25 mL). Isolated as a white solid (0.88 g, 88 %). ^{1}H NMR ($CDCl_3$) δ 6.64 (d, J = 4.5 Hz, 8H), 4.95 (d, J = 9.5 Hz, 6H), 4.53 (s, 2H), 3.97 – 3.90 (m, 7H), 3.87 (t, J = 6.4 Hz, 8H), 3.77 (t, J = 6.3 Hz, 3H), 1.79 – 1.72 (m, 18H), 1.52 – 1.50 (m, 4H), 1.48 – 1.41 (m, 14H), 1.36 – 1.28 (m, 144H), 0.91 (t, J = 6.7 Hz, 27H); ^{13}C NMR ($CDCl_3$) δ 153.34, 153.13, 152.96, 137.83, 137.80, 137.62, 137.34, 133.00, 132.31, 106.66, 106.26, 105.67, 75.31, 73.46, 73.37, 71.54, 69.14, 68.95, 67.96, 65.07, 32.10, 30.60, 30.57, 29.98, 29.96, 29.94, 29.92, 29.87, 29.83, 29.79, 29.76, 29.69, 29.64, 29.61, 29.57, 29.56, 26.40, 26.38, 26.35, 26.31, 22.84, 14.20; MALDI-TOF (m/z): $[M+Na]^+$ calcd. for $C_{136}H_{242}O_{13}Na$, 2106.82; found 2112.689.

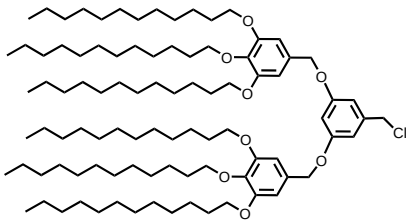

5,5'-(((5-(Chloromethyl)-1,3-phenylene)bis(oxy))bis(methylene))bis(1,2,3 tris(dodecyloxy)benzene), 2c. 2b (1.10 g, 0.77 mmol) was combined with 25 mL DCM and cooled to 0 °C before adding 2,6-ditert butyl 4-methyl pyridine (0.47 g, 2.31 mmol), then $SOCl_2$ (0.17 mL, 2.31 mmol). The reaction was warmed to room temperature and stirred for 3 hours under N_2 atm. The reaction mixture was then concentrated under vacuum, dissolved in $CHCl_3$ (100 mL) and washed with 1 M HCl (2 x 50 mL). The organic layer was dried with Na_2SO_4 and filtered before being concentrated under vacuum. **2c** was isolated as a yellow solid (0.98 g, 88 %). ^{1}H NMR ($CDCl_3$) δ 6.65 (s, 2H), 6.61 (s, 4H), 6.58 (s, 1H), 4.92 (s, 4H), 4.52 (s, 2H), 3.97 (q, J = 6.1 Hz, 12H), 1.82 – 1.74 (m, 12H), 1.47 (t, J = 7.5 Hz, 12H), 1.34 – 1.27 (m, 96H), 0.89 (t, J = 6.8 Hz, 18H); ^{13}C NMR ($CDCl_3$) δ 160.33, 153.53, 139.73, 138.30, 131.67, 107.86, 106.51, 102.30, 73.64, 70.82, 69.38, 46.51, 32.16, 32.14, 30.56, 29.97, 29.95, 29.92, 29.87, 29.84, 29.65, 29.61, 29.58, 26.36, 26.33, 22.90, 14.31; MALDI-TOF (m/z): $[M+Na]^+$ calcd. for $C_{93}H_{163}ClO_8Na$, 1466.19; found 1469.005.

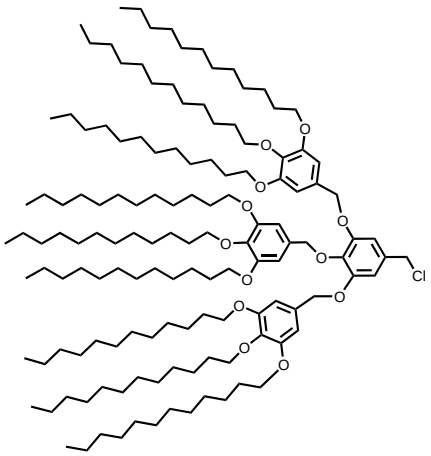

5,5',5''-(((5-(Chloromethyl)benzene-1,2,3-triyl)tris(oxy))tris(methylene))tris(1,2,3-tris(dodecyloxy)benzene), 3c. As for **2c**. **3b** (1.15 g, 0.56 mmol), 2,6-ditert butyl 4-methyl pyridine (0.34 g, 1.69 mmol), $SOCl_2$ (0.13 mL, 1.69 mmol), CH_2Cl_2 (25 mL). **3c** was isolated as a yellow solid (1.07 g, 91 %). ^{1}H NMR ($CDCl_3$) δ 6.69 (s, 2H), 6.62 (d, J = 5.2 Hz, 6H), 5.00 (s, 4H), 4.97 (s, 2H), 4.47 (s, 2H), 3.95 (t, J = 6.5 Hz, 5H), 3.88 (t, J = 6.3 Hz, 10H), 3.77 (t, J = 6.3 Hz, 3H), 1.78 – 1.71 (m, 18H), 1.50 – 1.43 (m, 18H), 1.33 – 1.27 (m, 144H), 0.89 (t, J = 6.2 Hz, 27H); ^{13}C NMR ($CDCl_3$) δ 153.37, 153.12, 153.06, 138.75, 137.97, 137.88, 133.11, 132.77, 132.01, 108.93, 107.16, 106.43, 105.82, 77.43, 75.32, 73.43, 73.36, 71.84, 69.15, 68.96, 58.30, 46.63, 37.45, 32.08, 32.07, 30.57, 30.54, 30.17, 29.95, 29.92, 29.89, 29.87, 29.84, 29.82, 29.79, 29.76, 29.73, 29.71, 29.63, 29.59, 29.54, 29.52, 29.50, 26.36, 26.32, 26.29, 22.81, 15.42, 14.19; MALDI-TOF (m/z): $[M+Na]^+$ calcd. for $C_{136}H_{241}ClO_{12}Na$, 2124.78; found 2130.649.

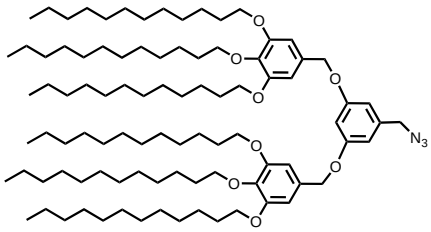

5,5'-(((5-(Azidomethyl)-1,3-phenylene)bis(oxy))bis(methylene))bis(1,2,3-tris(dodecyloxy)benzene), 2d. 2c (1.00 g, 0.69 mmol) was combined with NaN_3 (0.13 g, 2.08 mmol), and 30 mL DMF and was heated at 70 °C for 16 hours. The reaction mixture was cooled to room temperature and diluted in $CHCl_3$ (100 mL) then washed with water (2 x 50 mL). The organic layers were dried with Na_2SO_4, filtered, concentrated under vacuum, then the product was precipitated out of cold MeOH. **2d** was isolated as yellow solid (0.92 g, 92 %). ^{1}H NMR ($CDCl_3$) δ 6.61 (s, 4H), 6.59 (d, J = 2.2 Hz, 1H), 6.56 (d, J = 2.2 Hz, 2H), 4.92 (s, 4H), 4.27 (s, 2H), 3.99 – 3.93 (m, 12H), 1.81 – 1.73 (m, 12H), 1.49 – 1.44 (m, 12H), 1.34 – 1.26 (m, 96H), 0.90 – 0.86 (m, 18H); ^{13}C NMR ($CDCl_3$) δ 160.51, 153.56, 138.33, 137.83, 131.67, 107.41, 106.52, 102.07, 73.66, 70.84, 69.40, 55.09, 32.17, 32.15, 30.58, 29.99, 29.97, 29.93, 29.88, 29.85, 29.66, 29.62, 29.59, 26.37, 26.35, 26.32, 22.91, 14.33; MALDI-TOF (m/z): $[M+Na]^+$ calcd. for $C_{93}H_{163}N_3O_8Na$, 1473.23; found 1476.045.

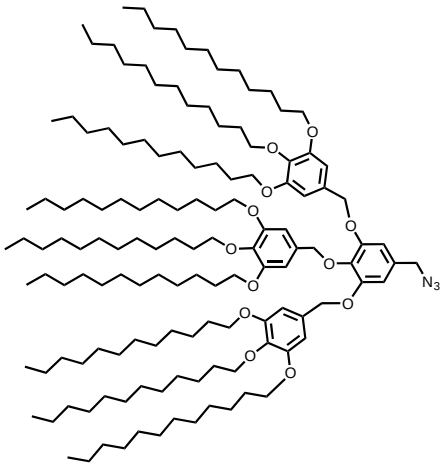

5,5',5''-(((5-(azidomethyl)benzene-1,2,3-triyl)tris(oxy))tris(methylene))tris(1,2,3-tris(dodecyloxy)benzene), 3d. As for **2d**. **3c** (1.50 g, 0.713 mmol), NaN_3 (0.14 g, 2.14 mmol), DMF (30 mL). **3d** was isolated as a yellow solid (1.44 g, 96 %). ^{1}H NMR ($CDCl_3$) δ 6.64 (d, J = 2.2 Hz, 6H), 6.62 (s, 2H), 5.02 (s, 4H), 5.00 (s, 2H), 4.22 (s, 2H), 3.96 (t, J = 6.7 Hz, 5H), 3.90 (t, J = 6.4 Hz, 10H), 3.80 (t, J = 6.3 Hz, 3H), 1.79 – 1.73 (m, 18H), 1.51 – 1.43 (m, 18H), 1.35 – 1.29 (m, 144H), 0.90 (t, J = 6.7 Hz, 27H); ^{13}C NMR ($CDCl_3$) δ 153.47, 153.31, 153.20, 138.68, 138.05, 137.97, 132.86, 132.09, 131.19, 108.52, 106.81, 106.51, 105.82, 75.41, 73.53, 73.46, 71.96, 69.33, 69.25, 69.06, 55.33, 55.09, 32.15, 32.13, 30.63, 30.60, 30.01, 29.98, 29.96, 29.94, 29.91, 29.88, 29.86, 29.83, 29.80, 29.77, 29.69, 29.65, 29.60, 29.58, 29.56, 26.42, 26.38, 26.35, 22.88, 14.27; MALDI-TOF (m/z): $[M+Na]^+$ calcd. for $C_{136}H_{241}N_3O_{12}Na$, 2131.82; found 2137.689.

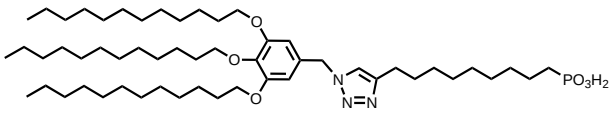

(9-(1-(3,4,5-Tris(dodecyloxy)benzyl)-1*H*-1,2,3-triazol-4-yl)nonyl)phosphonic acid, 1. Compound **1** was synthesized as reported previously.[2] 5-(azidomethyl)-1,2,3-tris(dodecyloxy)benzene (1.7 g, 2.50 mmol), 10-undeconoic phosphonic acid (0.5 g, 2.74 mmol), $CuSO_4 \cdot 5H_2O$ (cat), sodium ascorbate (cat), THF (3 mL), and H_2O (0.5 mL) were combined and stirred for 12 hours at 75 °C with microwave irradiation. The solution was diluted with $CHCl_3$ (100 mL) and washed with 4 M HCl (2 x 50 mL) then 1 M HCl (50mL), before being dried with Na_2SO_4, filtered, and concentrated under vacuum. The crude product was diluted in a small amount of $CHCl_3$ and precipitated out of cold MeOH as pure **1** as a white powder, yield (1.58 g, 69 %). ^{1}H NMR ($CDCl_3$) δ 10.43 (s, 2H), 7.24 (s, 1H), 6.44 (s, 2H), 5.36 (s, 2H), 3.91 (q, J = 7.0 Hz, 6H), 2.68 (t, J = 7.8 Hz, 2H), 1.79 – 1.71 (m, 8H), 1.65 – 1.59 (m, 4H), 1.49 – 1.41 (m, 8H), 1.33 – 1.25 (m, 54H), 0.87 (t, J = 6.7 Hz, 9H); ^{13}C NMR ($CDCl_3$) δ 153.79, 148.53, 138.74, 129.50, 121.16, 106.94, 73.67, 69.48, 54.85, 32.14, 30.55, 30.35, 30.22, 29.96, 29.95, 29.92, 29.90, 29.88, 29.86, 29.82, 29.65, 29.60, 29.58, 29.40, 29.18, 29.04, 29.00, 28.90, 27.08, 26.33, 26.32, 25.96, 25.46, 22.90, 22.40, 22.36, 14.31; MALDI-TOF (m/z): $[M+Na]^+$ calcd. for $C_{54}H_{100}N_3O_6PNa$, 940.724; found 941.825.

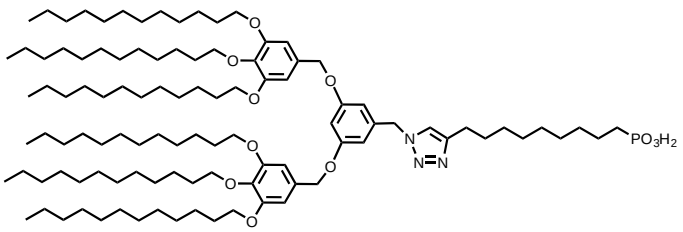

(9-(1-(3,5-Bis((3,4,5-tris(dodecyloxy)benzyl)oxy)benzyl)-1*H*-1,2,3-triazol-4-yl)nonyl)phosphonic acid, 2. As for **1**, **2d** (0.50 g, 0.34 mmol), 10-undeconoic phosphonic acid (0.09 g, 0.38 mmol), $CuSO_4 \cdot 5H_2O$ (cat), sodium ascorbate (cat), THF (3 mL), H_2O (0.5 mL), 16 hours at 75 °C under microwave irradiation. Isolated **2** as a yellow solid (0.35 g, 61 %). ^{1}H NMR ($CDCl_3$) δ 7.23 (s, 1H), 6.58 (s, 5H), 6.50 (s, 2H), 5.40 (s, 2H), 4.86 (s, 4H), 3.98 – 3.92 (m, 12H), 2.67 (t, J = 8.1 Hz, 2H), 1.82 – 1.71 (m, 16H), 1.65 – 1.61 (m, 2H), 1.49 – 1.42 (m, 14H), 1.35 – 1.26 (m, 106H), 0.89 – 0.86 (m, 18H); ^{13}C NMR ($CDCl_3$) δ 160.57, 153.47, 148.62, 138.19, 136.86, 131.39, 121.23, 107.26, 106.37, 102.17, 100.12, 73.58, 70.76, 69.27, 54.47, 32.12, 32.10, 30.53, 29.94, 29.92, 29.89, 29.84, 29.81, 29.62, 29.60, 29.58, 29.55, 29.37, 29.20, 29.04, 28.87, 26.32, 25.44, 22.87, 14.28; MALDI-TOF (m/z): $[M+Na]^+$ calcd. for $C_{104}H_{184}N_3O_{11}PNa$, 1705.36; found 1708.284.

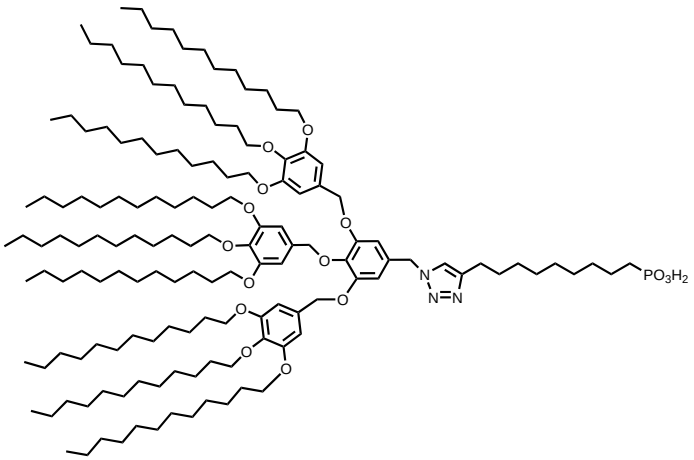

(9-(1-(3,4,5-Tris((3,4,5-tris(dodecyloxy)benzyl)oxy)benzyl)-1*H*-1,2,3-triazol-4-yl)nonyl)phosphonic acid, 3. As for **1**, **3d** (0.30 g, 0.14 mmol), 10-undeconoic phosphonic acid (0.04 g, 0.16 mmol), $CuSO_4 \cdot 5H_2O$ (cat), sodium ascorbate (cat), THF (3 mL), H_2O (0.5 mL), 20 hours at 75 °C under microwave irradiation. Isolated **3** as a yellow solid (0.20 g, 62 %). ^{1}H NMR ($CDCl_3$) δ 7.17 (s, 1H), 6.58 (d, J = 13.8 Hz, 8H), 5.35 (s, 2H), 4.95 (s, 6H), 3.92 (t, J = 6.5 Hz, 5H), 3.86 (t, J = 6.4 Hz, 10H), 3.74 (t, J = 6.4 Hz, 3H), 2.68 (s, 2H), 1.74 – 1.63 (m, 21H), 1.48 – 1.39 (m, 21H), 1.31 – 1.24 (m, 154H), 0.88 (t, J = 6.8 Hz, 27H); ^{13}C NMR ($CDCl_3$) δ 153.54, 153.50, 153.28, 139.31, 138.08, 138.03, 132.75, 131.85, 129.44, 108.77, 106.41, 105.87, 75.44, 73.61, 73.54, 71.96, 69.32, 69.11, 32.17, 32.16, 30.67, 30.66, 30.05, 30.03, 30.01, 29.98, 29.95, 29.92, 29.88, 29.83, 29.75, 29.71, 29.68, 29.63, 29.61, 29.04, 28.92, 28.77, 28.66, 26.48, 26.45, 26.42, 22.92, 14.32; MALDI-TOF (m/z): $[M+Na]^+$ calcd. for $C_{147}H_{262}N_3O_{15}PNa$, 2363.965; found 2369.834.

Additional Figures and Microscopy

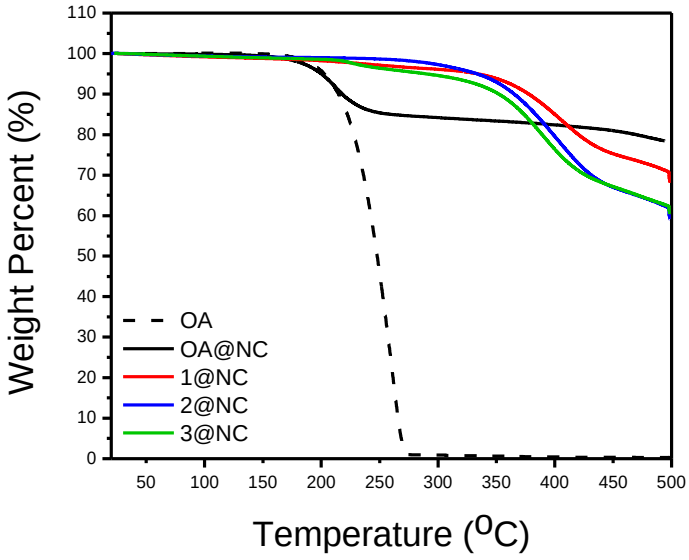

Figure S1. TGA of the NCs functionalized with OA and the dendrimer ligands, highlighting successful ligand exchange, due to change in observed thermal decomposition of ligands from about 190 °C to above 300 °C.

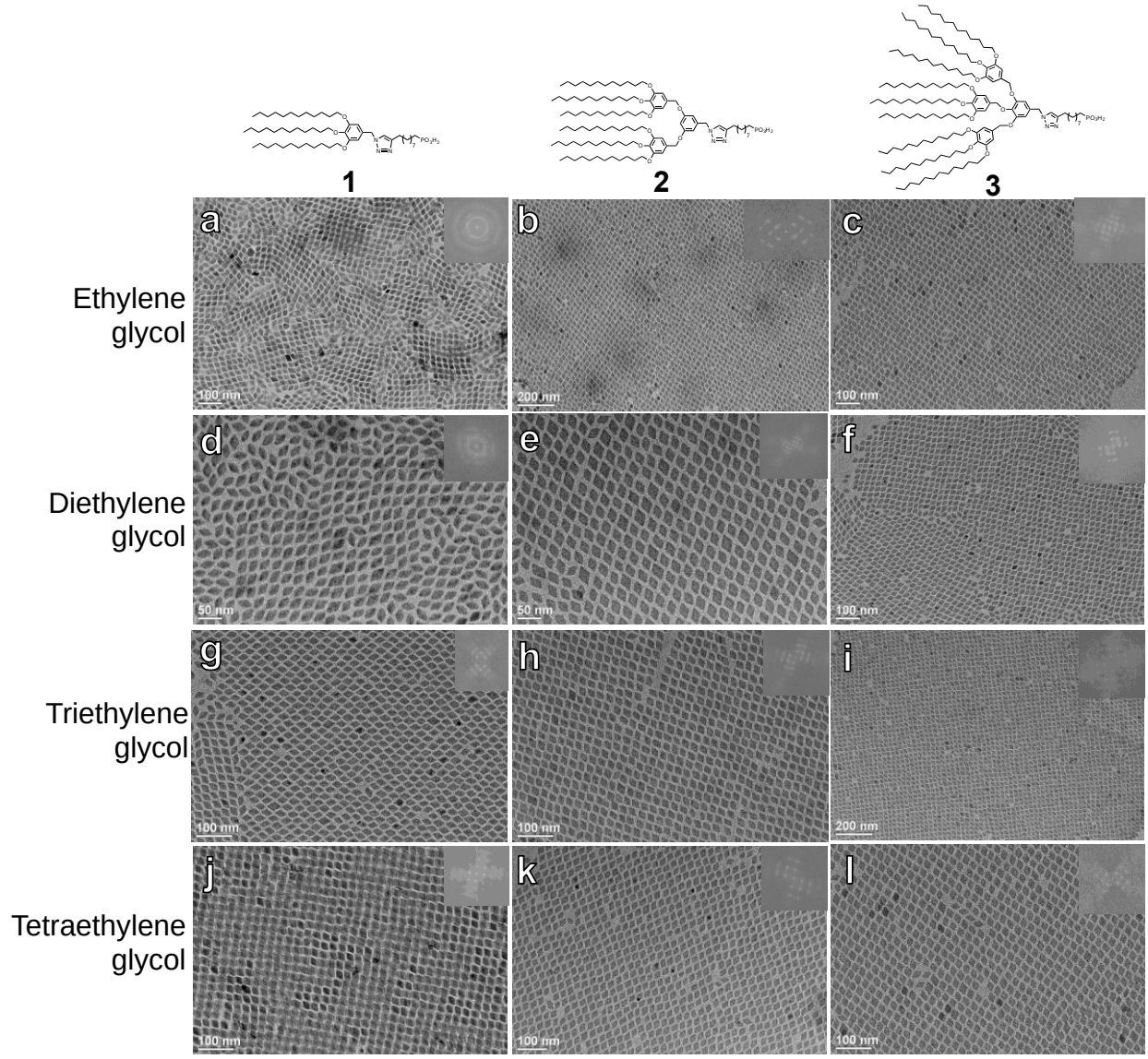

Figure S2. TEM images of self-assembled mono or bilayers on various subphases for each dendritic ligand.

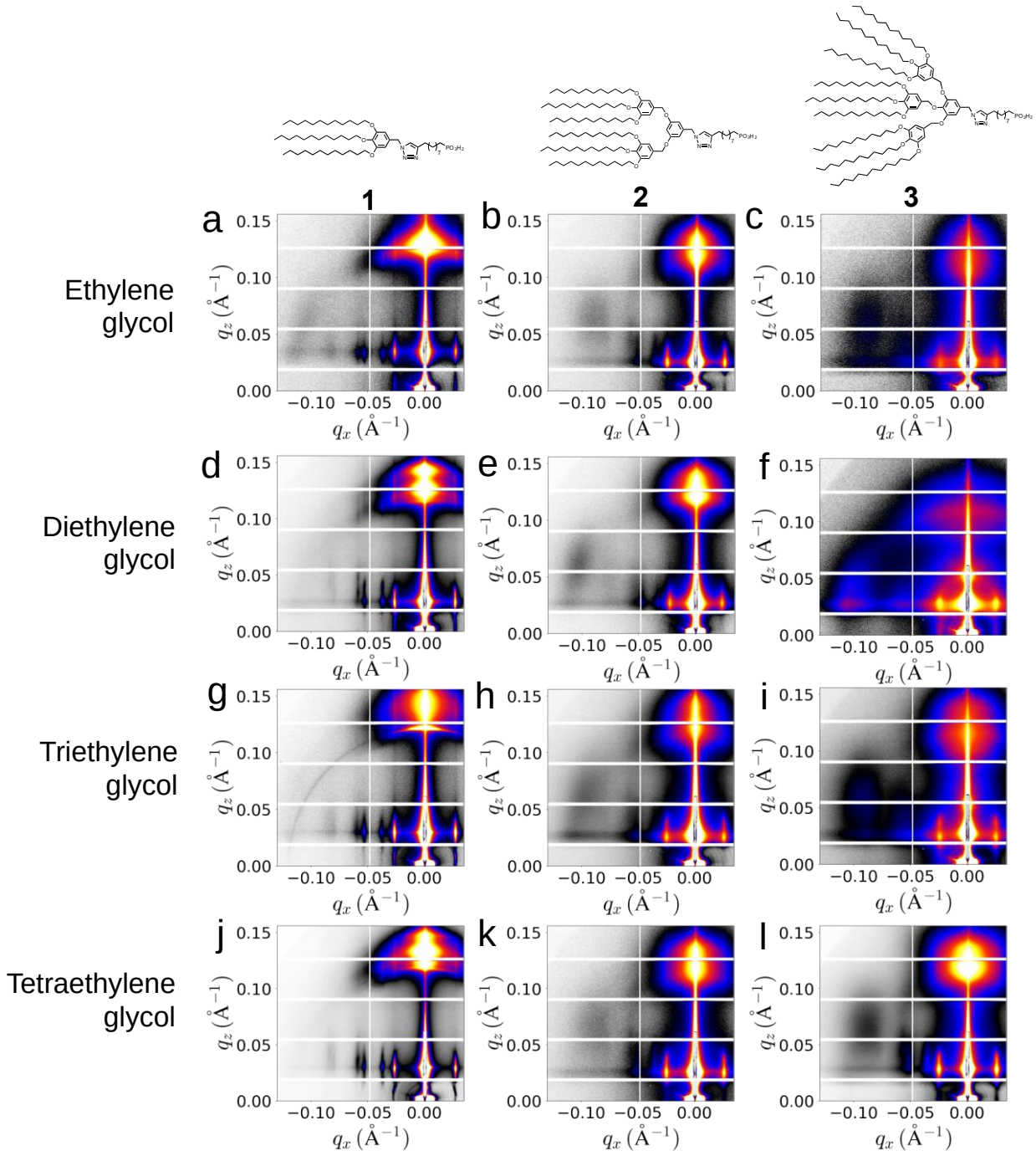

Figure S3. 2D GISAXS images of self-assembled mono or bilayers on various subphases for each dendritic ligand. Data was converted into reciprocal-space, including correction for Ewald sphere curvature. Data is displayed as the (q_x, q_z) projection (where the q_y component is ignored for plotting purposes).

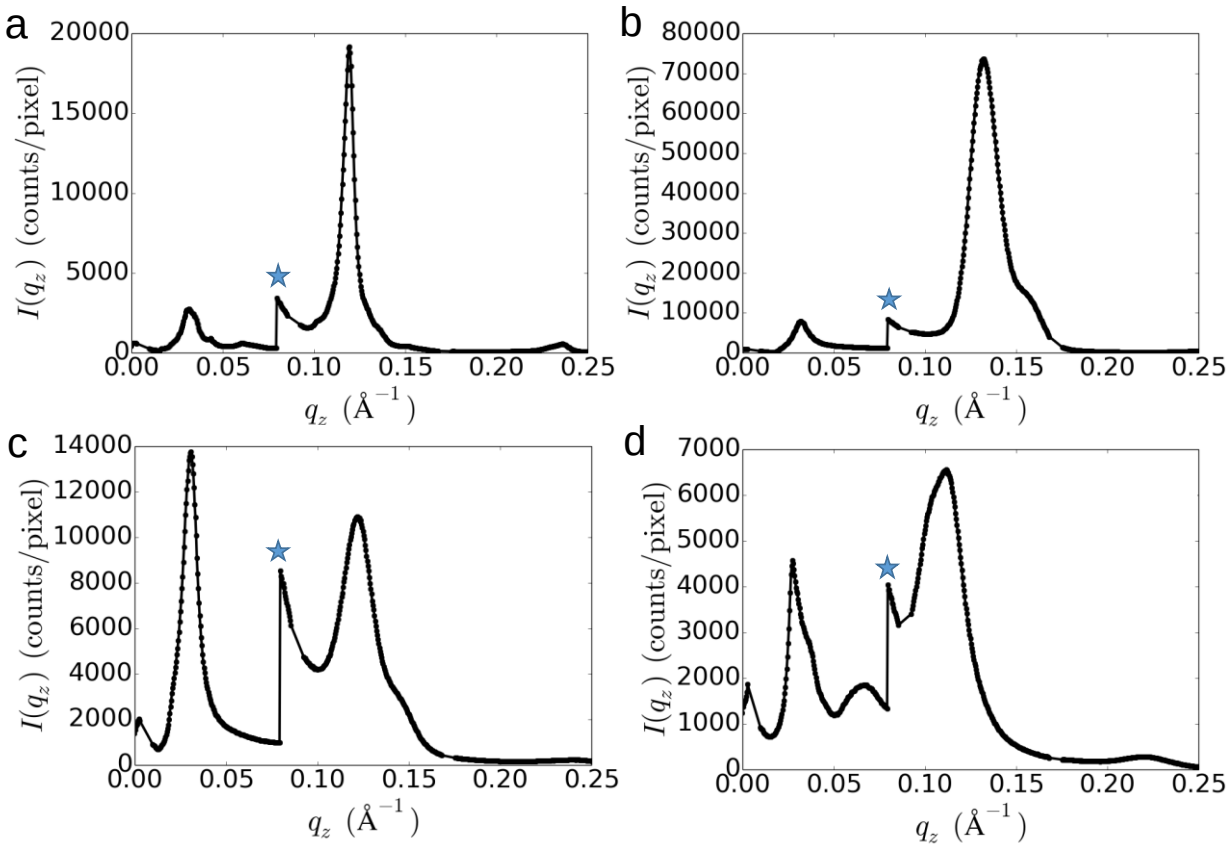

Figure S4. Linecuts along the out-of-plane (q_z) direction obtained from GISAXS for (a) **OA**@NC, (b) **1**@NC, (c) **2**@NC, and (d) **3**@NC. The discontinuity at q_z =0.08 Å^{-1} (marked by a star) appears due to the beamstop, which affects the range of pixels used in data averaging.

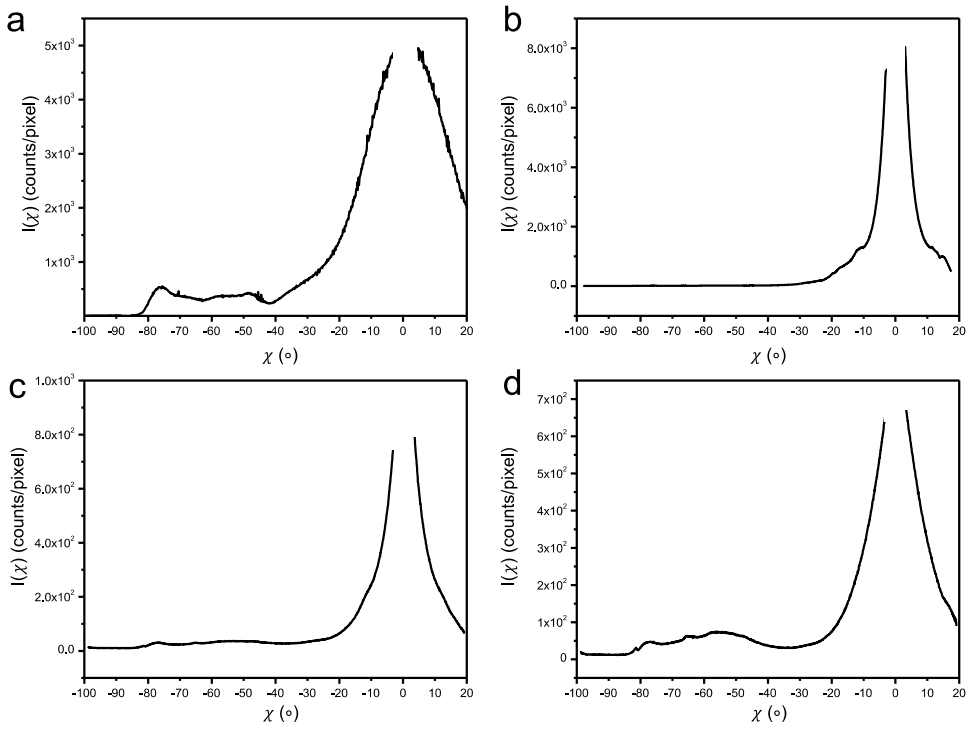

Figure S5. Angle (azimuthal) linecuts extracted from GISAXS for (a) **OA**@NC, (b) **1**@NC, (c) **2**@NC, and (d) **3**@NC. Data was extracted along the angular direction at a constant q corresponding to the most intense peak along q_z (q of 0.110 Å^{-1} to 0.130 Å^{-1}, depending on material).

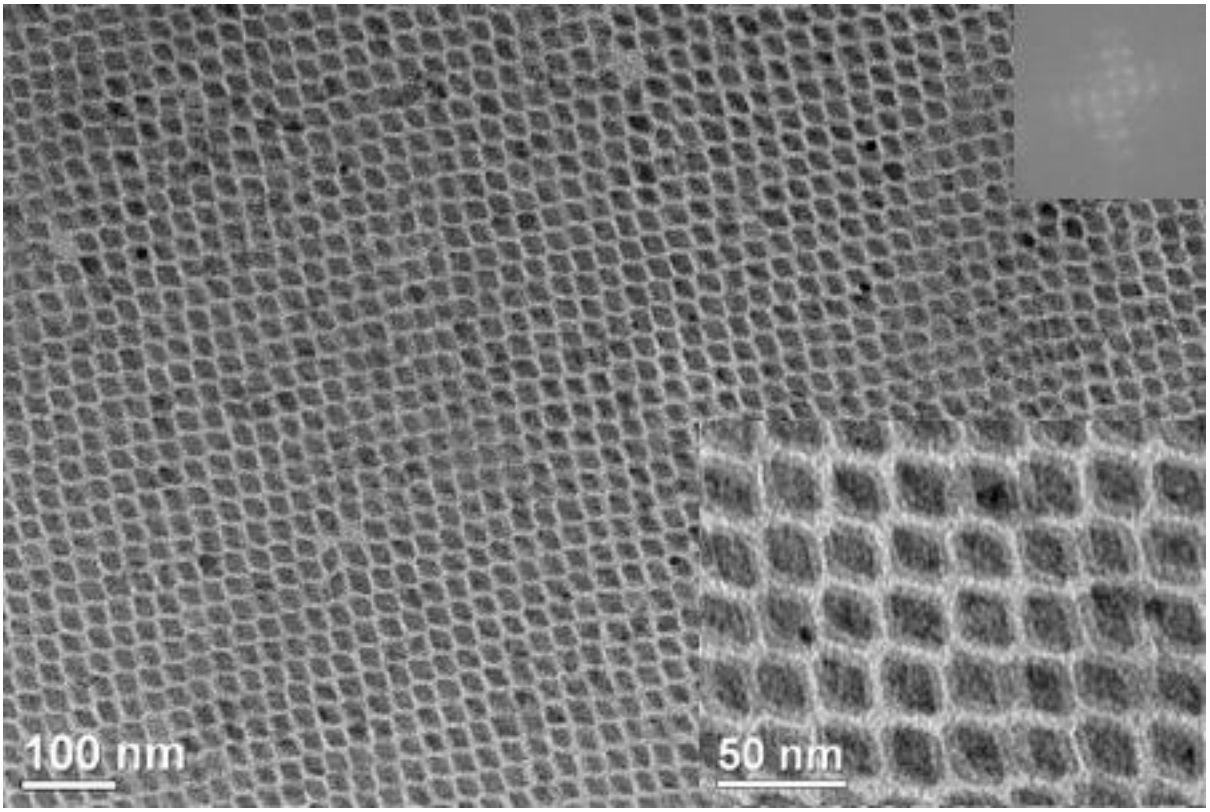

Figure S6. Large area view of bilayer film of **1**@NC.

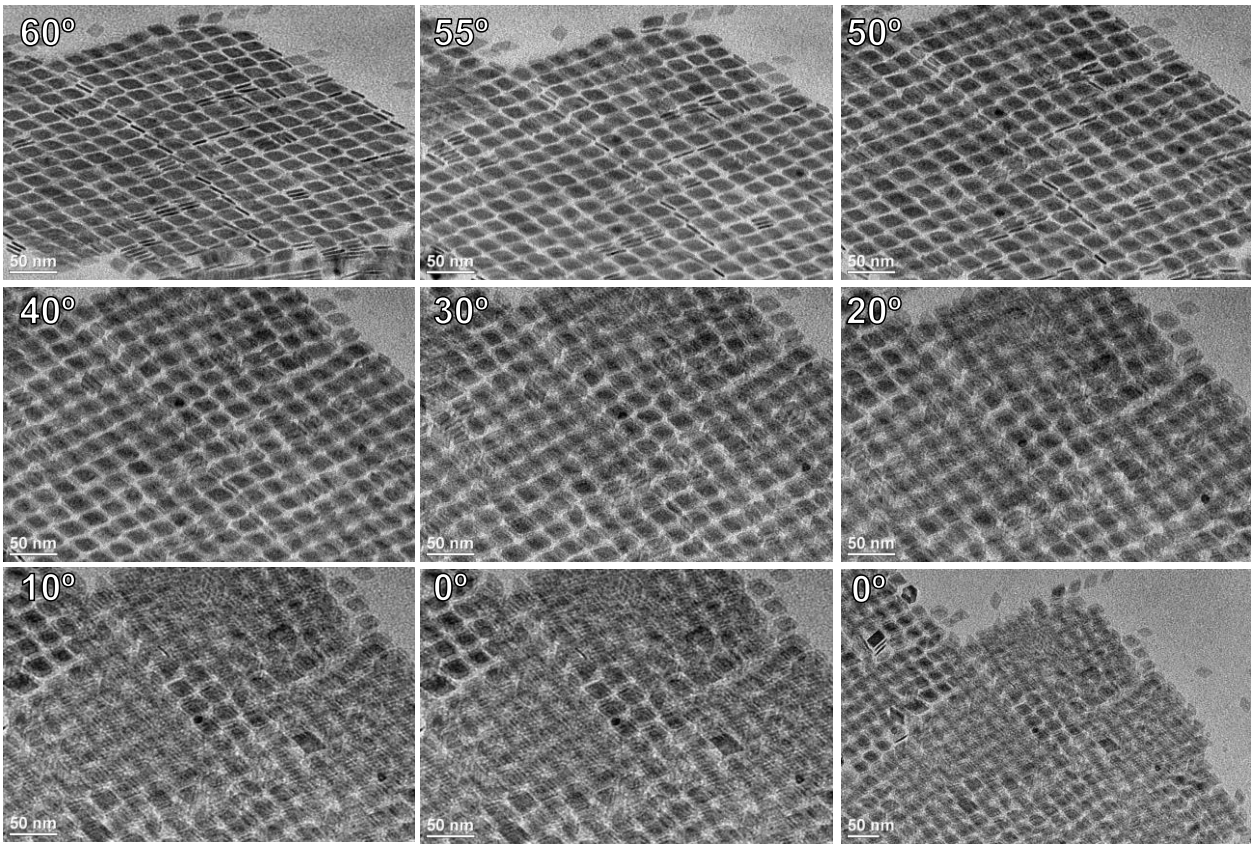

Figure S7. TEM tilt tomography of multilayer film of **3**@NC.

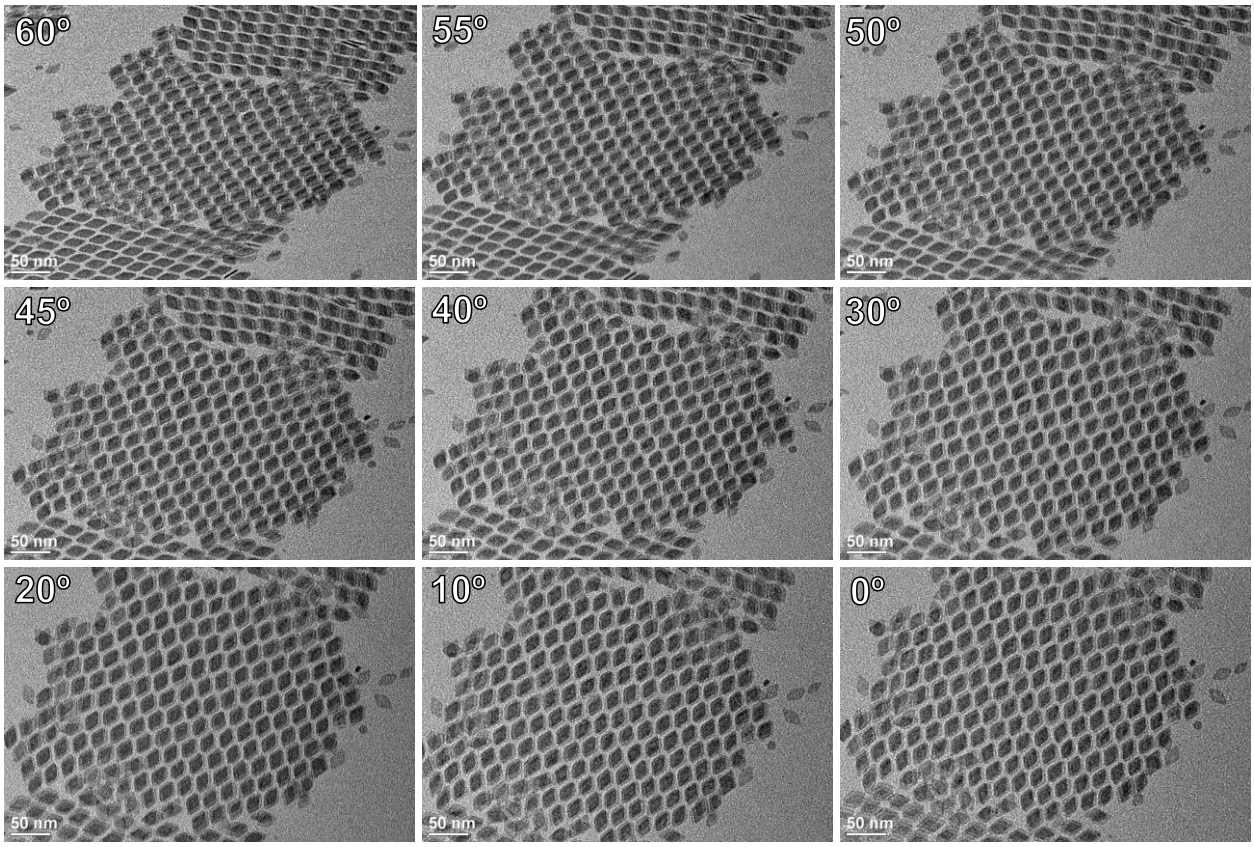

Figure S8. TEM tilt tomography of bilayer film of **2**@NC.

Scaling Theory for Branching Ligand Architecture

We provide a detailed derivation of a generalized scaling law for branching graft architecture. We start with the scaling relations for the end-to-end distance for non-grafted branching chains in both a good and theta solvent as shown in Eq. I.1 and I.2, respectively.[3,4]

$$R \sim N^{5/2(d+2)} \Lambda^{-1/2(d+2)} v^{1/(d+2)} \tag{I.1}$$

$$R \sim N^{7/4(d+1)} \Lambda^{(5-2d)/4(d+1)} \tag{I.2}$$

where R is the end-to-end distance, N is the chain length, Λ is the branching activity, v is the excluded volume of the chain's statistical segment, and d is the dimensionality. Here, Λ is defined such that $N\Lambda = 1$ converges to the linear chain limit. We are interested in the 3D limit to capture our experimental systems. For $d = 3$, Eq. I.1 and I.2 become:

$$R \sim N^{1/2} \Lambda^{-1/10} v^{1/5} \tag{I.3}$$

$$R \sim N^{7/16} \Lambda^{-1/16} \tag{I.4}$$

As a consistency check, in the limit of a linear chain, $\Lambda \sim N^{-1}$ and Eq. I.3 and I.4 converge to the well known good and theta scaling behavior for linear chains – $R \sim N^{3/5} v^{1/5}$ and $R \sim N^{1/2}$, respectively.

Using Eq. I.3 and I.4, we now define a parameter $\alpha = R_{good}/R_{theta}$ that measures how much a chain swells relative to its equilibrium conformation when placed in a good solvent environment.

$$\alpha^5 \sim N^{1/2} v [N\Lambda]^{-3/16} \tag{I.5}$$

Again, Eq. I.5 converges to its linear chain analog of $\alpha \sim N^{1/2} v$ when $N\Lambda = 1$. In general, values for $N\Lambda$ are always greater than 1 for branching chains. Thus, by inspection, it is immediately clear that branching reduces the amount a chain of length N can swell relative to its linear counterpart. This is a direct manifestation of junctions along a branching chain's backbone that place physical constraints on how much a local segment can swell.

The above results are for free chains in solution. To bridge Eq. I.1 - I.5 to the grafting limit, we utilize an analogous scaling argument employed by Vo *et al*.[5] for linear grafts on the surface of anisotropic particles. Again, we define three relevant regimes for chain behavior as a function of the radial distance r away from the grafting surface – swollen (semi-dilute), un-swollen (theta), and stretched (flat-brush).

We start with the radial region around the core where chains are swollen. In this limit, the chain swells due to favorable interactions with the solvent and we can apply Eq. I.5 in conjunction with the constraint that local and global monomer volume fraction within a layer r must be equal to give:

$$\xi(r) \sim r f^{-1/2} \Omega^{3/2} \tag{I.6}$$

$$n(r) \sim \left(\frac{r}{b}\right)^2 f^{-1}\nu^{-2/5}\Omega^3\Lambda^{1/5} \tag{I.8}$$

$$\psi(r) \sim \left(\frac{r}{b}\right)^{-1} f^{1/2}\nu^{-2/5}\Omega^{-3/2}\Lambda^{1/5} \tag{I.9}$$

where ξ is the correlation blob size, n is the number of monomers, ψ is the volume fraction, b is the kuhn length, and f is the number of grafts and is related to the grafting density σ *via* the relation $\sigma \sim f/r_o^2$ with r_o representing the in-sphere radius of the shape of interest. In order to keep Eq. I.6 - I.9 generalized for an arbitrary core shape, we introduced the parameter $\boldsymbol{\Omega}$ that defines both the shape and specific position on the particle surface.

As we move radially inward, there exists a cross-over value of r_θ where the local monomer concentration is high enough that no additional solvent can penetrate into the brush layer. At this point, chains can no longer swell due to solvent interaction and must relax back to their theta conformation. The transition value of r_θ can be directly solved for by setting $\alpha(r) \sim 1$ in Eq. I.7 to give

$$r_\theta \sim bf^{1/2}\nu^{-7/5}\Omega^{-3/2}\Lambda^{1/5} \tag{I.10}$$

Enforcing $\alpha(r) = 1$ also enables us to derive the analog of Eqs. I.6 and I.8 - I.9 for the theta regime:

$$\xi(r) \sim rf^{-1/2}\boldsymbol{\Omega}^{3/2} \tag{I.11}$$

$$n(r) \sim \left(\frac{r}{b}\right)^{16/7} f^{-8/7}\Omega^{24/7}\Lambda^{1/7} \tag{I.12}$$

$$\psi(r) \sim \left(\frac{r}{b}\right)^{-5/7} f^{5/14}\Omega^{15/14}\Lambda^{1/7} \tag{I.13}$$

Moving further radially inward, we will eventually hit another cross-over value of r_c where the chains are so confined that they are forced to fully extend to an all-*trans* conformation. In this fully-stretched limit, the monomer concentration becomes uniform. Setting $\psi(r) \sim 1$ in Eq. I.13 allows for us to solve for r_c to be

$$r_c \sim bf^{1/2}\Omega^{-3/2}\Lambda^{1/5} \tag{I.14}$$

Knowing $\psi(r) \sim 1$ and $\alpha(r) \sim 1$ trivially makes $\xi(r) \sim b$ and $n(r) \sim 1$ for the stretched regime. Table I.1 and Eq. I.15 provide a summary of the derived scaling behavior in the various regimes along with the cross-over distances.

Table SI 1: Scaling Behavior for Anisotropic Grafting

	Swollen	Theta	Stretched
$\xi(r)$	$r\Omega^{3/2}f^{-1/2}$	$r\Omega^{3/2}f^{-1/2}$	b
$n(r)$	$r^2f^{-1}\nu^{-2/5}\Omega^3\Lambda^{1/5}b^{-2}$	$r^{16/7}f^{-8/7}\Omega^{24/7}\Lambda^{1/7}b^{-16/7}$	1
$\psi(r)$	$r^{-1}f^{1/2}\nu^{-2/5}\Omega^{-3/2}\Lambda^{1/5}b$	$r^{-5/7}f^{5/14}\Omega^{15/14}\Lambda^{1/7}b^{5/7}$	1
$\alpha(r)$	$r^{1/8}f^{-1/16}\nu^{7/40}\Omega^{3/16}\Lambda^{-1/40}b^{-1/8}$	1	1

$$\begin{array}{lcccl} \text{Swollen:} & & r & > & bf^{1/2}\nu^{-7/5}\Omega^{-3/2}\Lambda^{1/5} \\ \text{Unswollen:} & bf^{1/2}\Omega^{-3/2}\Lambda^{1/5} < & r & < & bf^{1/2}\nu^{-7/5}\Omega^{-3/2}\Lambda^{1/5} \\ \text{Core:} & & r & < & bf^{1/2}\Omega^{-3/2}\Lambda^{1/5} \end{array} \quad \text{(I.15)}$$

In order to predict the corona size that results from grafting we integrate the $\psi(r)$ across all relevant regimes as follows

$$Nfb^3\int_0^R \phi(r)d\vec{r}$$

where N is the total chain length, R is the center-to-chain distance of interest, and $d{\sim}r \sim r^2\Omega^3 dr$. Expanding over the relevant regimes gives:

$$Nfb^3 \sim \int_0^{r_c} r^2\Omega^3 dr + \int_{r_c}^{r_\theta} b^{5/7}f^{5/14}\Omega^{57/14}r^{9/7}dr + \int_{r_\theta}^{R} bf^{1/2}\nu^{-2/5}\Omega^{3/2}\Lambda^{1/5}rdr \quad \text{(I.16)}$$

Integrating and grouping terms give

$$R^2 \sim Nb^2f^{1/2}\nu^{2/5}\Omega^{-3/2}\Lambda^{-1/5} + b^2f^{13/14}\nu^{2/5}\Omega^{-6/7}\Lambda^{9/35}\left(\Omega^{48/7}-\nu^{-16/5}\right) + b^2f\nu^{2/5}\Omega^{-3}\Lambda^{-1/5}\left(\nu^{-16/5}-1\right) \quad \text{(I.17)}$$

We are interested only in the dominant term in N. Dropping all other terms gives

$$R \sim N^{1/2}bf^{1/4}\nu^{1/5}\Omega^{-3/4}\Lambda^{-1/10} \quad \text{(I.18)}$$

In its current form, Eq. I.18 is hard to directly compare with the linear grafting result. To better facilitate comparison, we can rewrite it as:

$$R \sim r_o\sigma^{1/5}\nu^{1/5}b^{2/5}\left[\frac{N}{\Omega}\frac{b}{r_o}\right]^{3/5}\left[\frac{r_o\sigma^{1/2}}{N\Lambda\Omega^{3/2}}\right]^{1/10} \quad \text{(I.19)}$$

For a linear chain, the corona size is:

$$R \sim r_o \sigma^{1/5} \nu^{1/5} b^{2/5} \left[\frac{N}{\Omega} \frac{b}{r_o} \right]^{3/5} \tag{I.20}$$

By inspection, we gain a factor of $\left[\frac{r_o \sigma^{1/2}}{N\Lambda\Omega^{3/2}}\right]^{1/10}$ in the branching result. Note here that convergence to the linear limit is now convoluted by both the effect of grafting ($r_o\sigma^{1/2}$) and of the core shape ($\Omega^{3/2}$). As a result, rather than $N\Lambda \sim 1$ resulting in a linear chain in the free chain limit, we get $N\Lambda \sim r_o\sigma^{1/2}\Omega^{-3/2}$. Eq. I.19 gives us a way to directly compare the effect of branching versus linear chains. From Eq. I.5, we noted that branching alters the degree of swelling a chain experiences. This is analogous to rescaling the kuhn length b of the chain. Thus, we can group the extra factor together with the $b^{2/5}$ dependency in both Eq. I.19 and I.20 to give

$$b_{branch} \sim b_{linear} \left[\frac{r_o \sigma^{1/2}}{N\Lambda\Omega^{3/2}} \right]^{1/4} \tag{I.21}$$

Setting $\Omega \sim 1$ to remove the effect of core shape gives the kuhn length rescaling employed in the main text. Lastly, we can define the free energy for the chain

$$\frac{F}{kT} \sim \frac{R^2}{N^{7/16}\Lambda^{-1/16}} + \nu \frac{N^2 f}{(\Omega R)^3} \tag{I.22}$$

This free energy can then be used as a Boltzmann weighting factor to determine the probability P of grafting to various locations on the surface of any arbitrarily defined anisotropic particle. Eq. I.23 defines the partitioning probability and will be heavily utilized to understand how corona morphology drives self-assembly as well as for mapping our theoretical predictions to simulation.

$$P \sim \frac{\exp(-F/kT)}{\iiint \exp(-F/kT) d\vec{r}} \tag{I.23}$$

Mapping of Scaling Prediction to Simulation

Here, we provide an example of how we mapped the theoretical scaling results from the previous section to a set of parameters for use in simulation. We first compute the partitioning probability of ligands on the surface of the nanoplate. This is performed *via* generating grid points on the particle surface and computing P from Eq. I.23 at each point. A set of potential mean forces was then computed between two grafted particles using P as an additional weighting probability of for interactions between each point on the particles' surface. While exact, creating a unique bead type for each point the particle surface become prohibitively expensive for a molecular dynamics simulations (Fig. S9a). In order to reduce the complexity of the simulation model, we categorize the continuous probability distribution into 3 distinct group based on the value, P, of the scaled grafting probabilities: low for $P \in [0,0.33)$, medium for $P \in [0.33,0.5)$, and high for $P \in [0.5,1]$ (Fig. S9b). Potential mean forces for surface points falling within each probability range are then averaged together to give an effective potential of interaction that can be readily employed in simulation (Fig. S9c). We then create a rigid body of smaller surface beads that sit on the nanoplate and attribute interaction strengths to each bead based on the bead type (red, blue, or green) for used in simulation. Standard mixing rules apply for cross interactions between particle types.

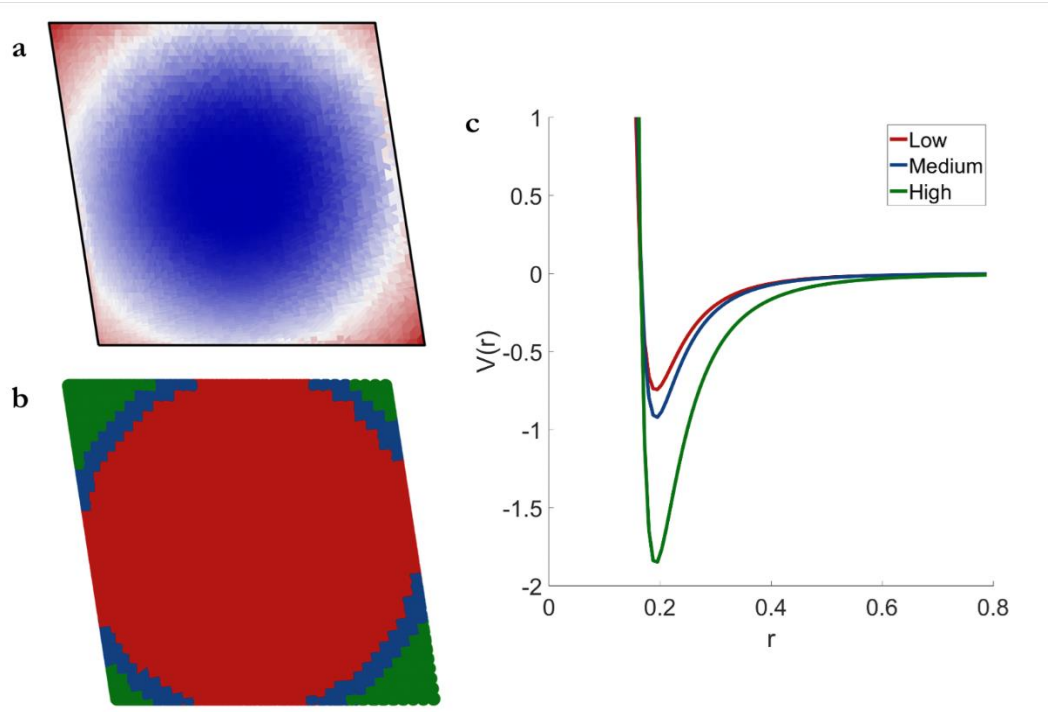

Figure S9. Mapping of Scaling Theory to Simulation. a). Original partitioning probabilities for ligand to surface nanoplate. b). Categorization of surface points based on bracketing range for partitioning probabilities (low: red, medium: blue, and high: green). c). Averaged potential mean force computed from surface point interactions for each bracketing range used simulation.

References

(1) Elbert, K. C.; Jishkariani, D.; Wu, Y.; Lee, J. D.; Donnio, B.; Murray, C. B. Design, Self-Assembly, and Switchable Wettability in Hydrophobic, Hydrophilic, and Janus Dendritic Ligand–Gold Nanoparticle Hybrid Materials. *Chem. Mater.* **2017**, *29*, 8737–8746.

(2) Diroll, B. T.; Jishkariani, D.; Cargnello, M.; Murray, C. B.; Donnio, B. Polycatenar Ligand Control of the Synthesis and Self-Assembly of Colloidal Nanocrystals. *J. Am. Chem. Soc.* **2016**, *138*, 10508–10515.

(3) Daoud, M.; Joanny, J. F. Conformation of Branched Polymers. *J. Phys.* **1981**, *42*, 1359–1371.

(4) Zimm, B. H.; Stockmayer, W. H. The Dimensions of Chain Molecules Containing Branches and Rings. *J. Chem. Phys.* **1949**, *17,* 1301–1314.

(5) Lu, F.; Vo, T.; Zhang, Y.; Frenkel, A.; Yager, K. G.; Kumar, S.; Gang, O. Unusual Packing of Soft-Shelled Nanocubes. *Sci. Adv.* **2019**, *5*, eaaw2399.

Copies of ^{1}H and ^{13}C spectra

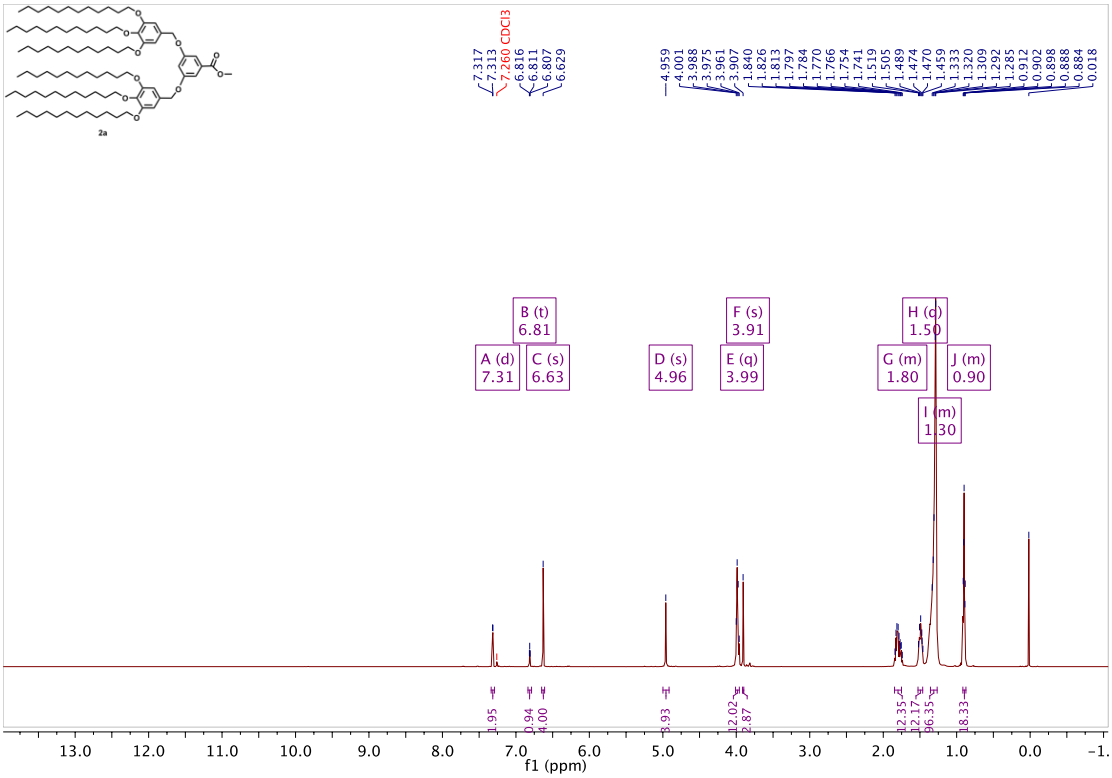

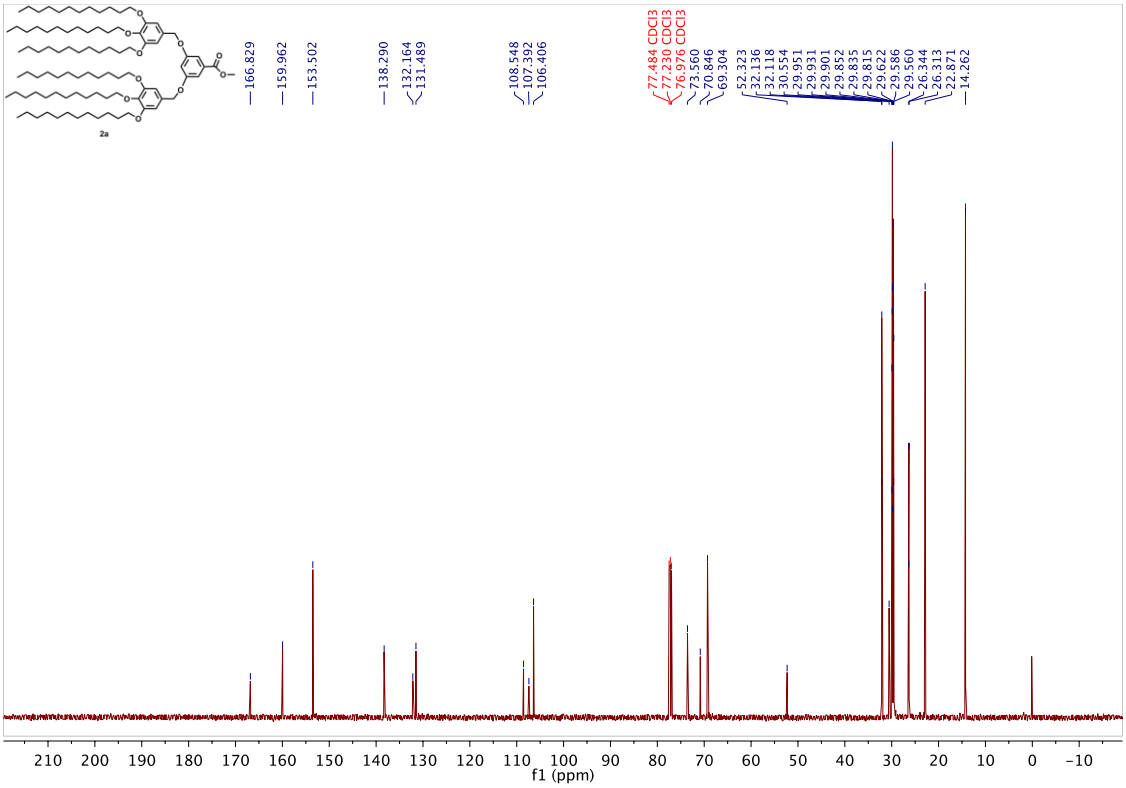

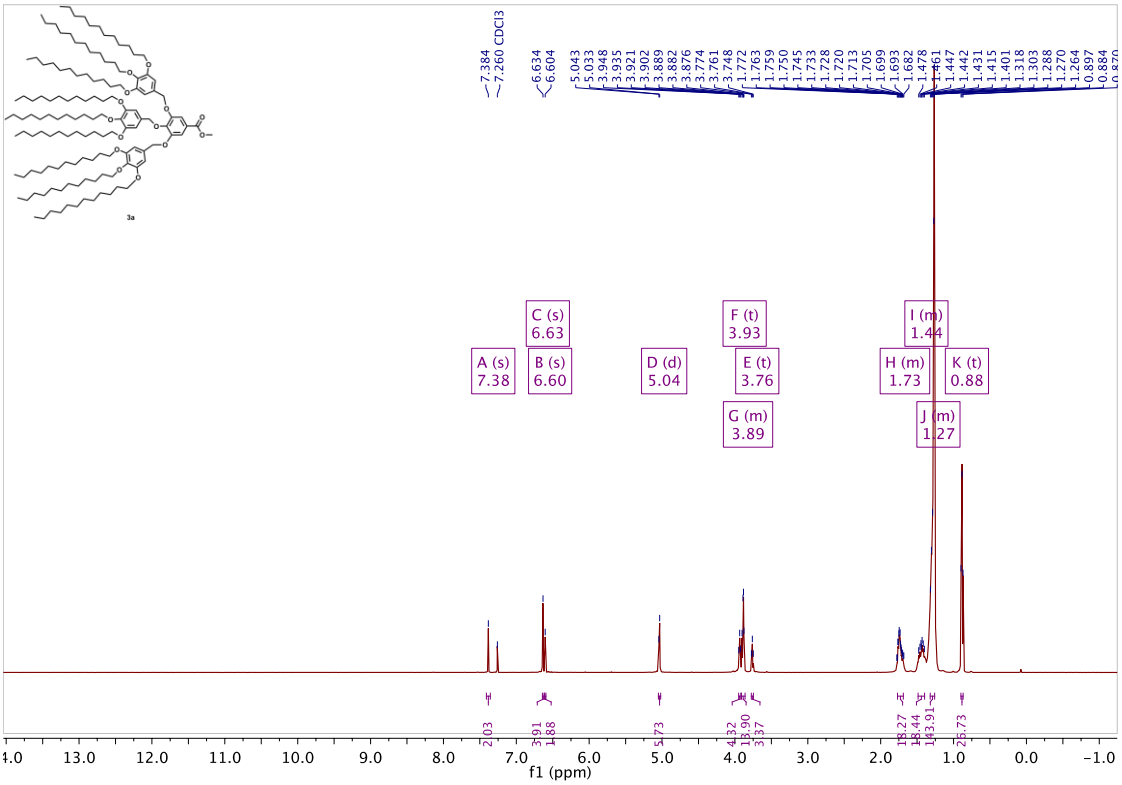
7.384
7.260 CDCl3
6.634
6.604
5.043
5.033
3.948
3.935
3.921
3.902
3.889
3.882
3.876
3.774
3.761
3.748
1.772
1.763
1.759
1.750
1.745
1.733
1.728
1.720
1.713
1.705
1.699
1.693
1.682
1.478
1.461
1.447
1.442
1.431
1.415
1.401
1.318
1.303
1.288
1.270
1.264
0.897
0.884
A (s) 7.38
B (s) 6.60
C (s) 6.63
D (d) 5.04
E (t) 3.76
F (t) 3.93
G (m) 3.89
H (m) 1.73
I (m) 1.44
J (m) 1.27
K (t) 0.88
2.03
3.91
1.88
5.73
4.32
13.90
3.37
18.27
18.44
143.91
26.73
f1 (ppm)

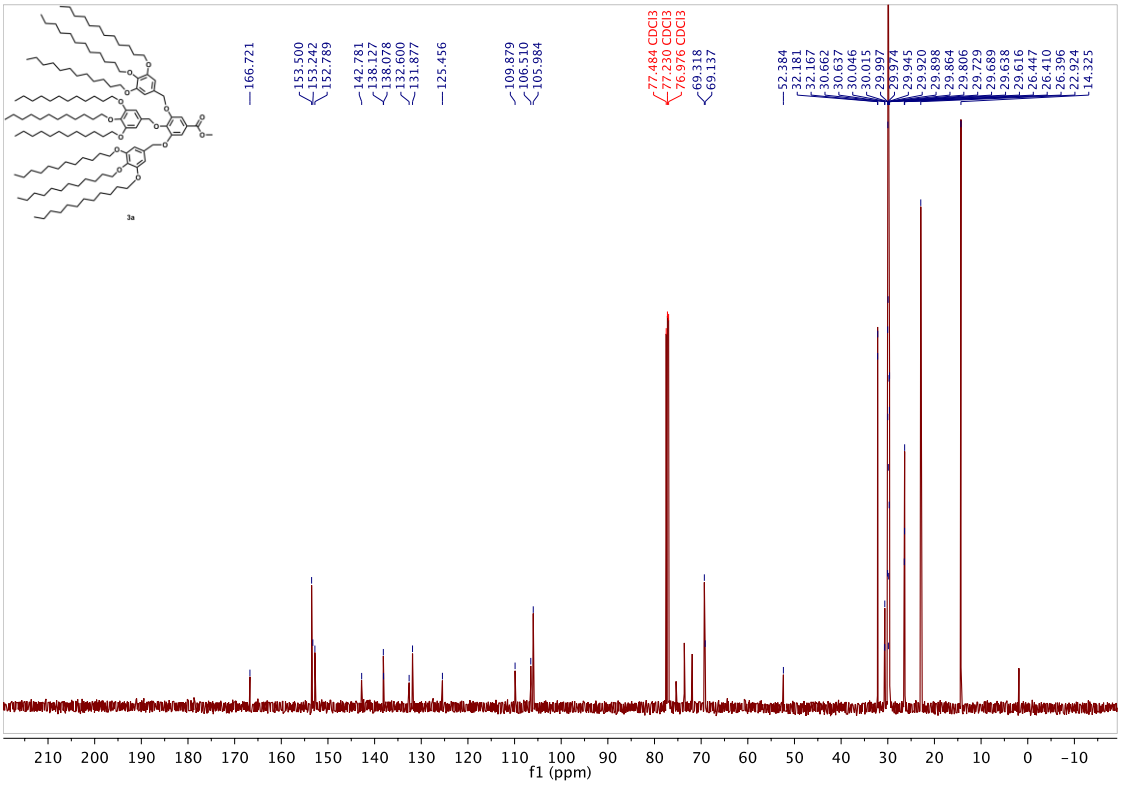
166.721
153.500
153.242
152.789
142.781
138.127
138.078
132.600
131.877
125.456
109.879
106.510
105.984
77.484 CDCl3
77.230 CDCl3
76.976 CDCl3
69.318
69.137
52.384
32.181
32.167
30.662
30.637
30.046
30.015
29.997
29.974
29.945
29.920
29.898
29.864
29.806
29.729
29.689
29.638
29.616
26.447
26.410
26.396
22.924
14.325
f1 (ppm)

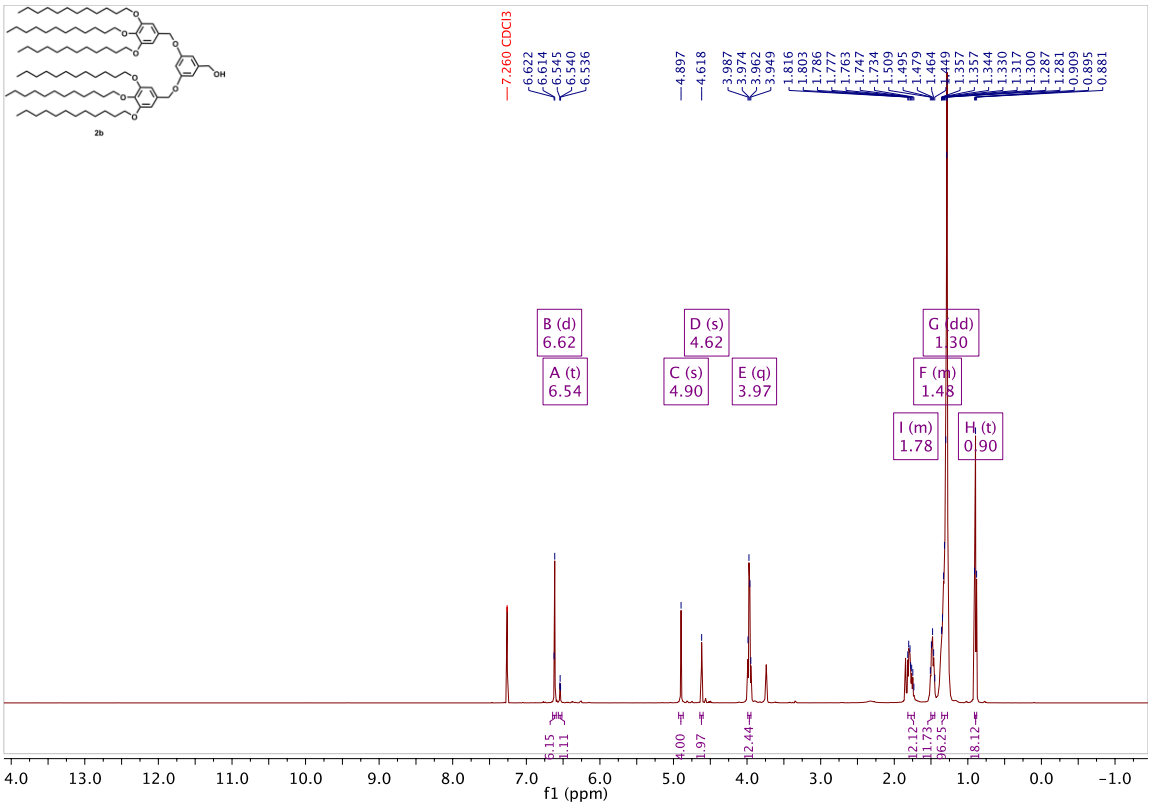
7.260 CDCl3
6.622
6.614
6.545
6.540
6.536
4.897
4.618
3.987
3.974
3.962
3.949
1.816
1.803
1.786
1.777
1.763
1.747
1.734
1.509
1.495
1.479
1.464
1.449
1.357
1.357
1.344
1.330
1.317
1.300
1.287
1.281
0.909
0.895
0.881
B (d) 6.62
A (t) 6.54
D (s) 4.62
C (s) 4.90
E (q) 3.97
G (dd) 1.30
F (m) 1.48
I (m) 1.78
H (t) 0.90
3.15
1.11
4.00
1.97
12.44
12.12
11.73
36.25
18.12
f1 (ppm)

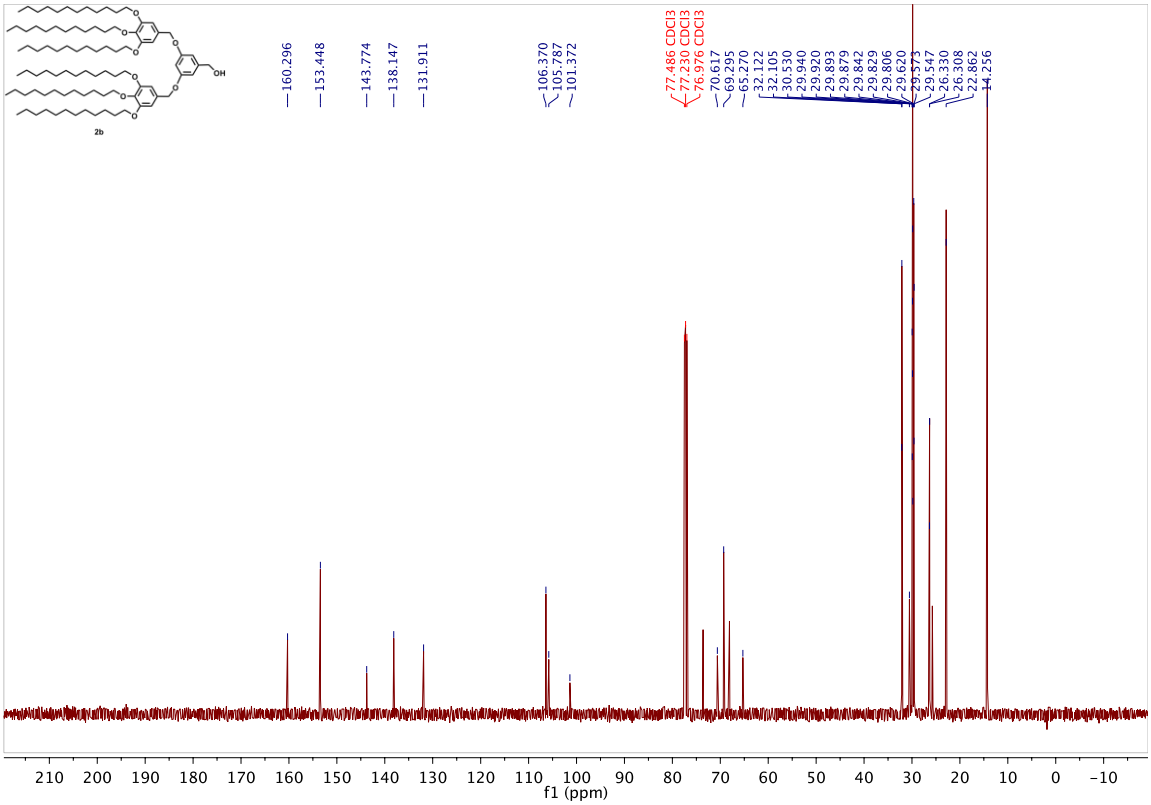
160.296
153.448
143.774
138.147
131.911
106.370
105.787
101.372
77.486 CDCl3
77.230 CDCl3
76.976 CDCl3
70.617
69.295
65.270
32.122
32.105
30.530
29.940
29.920
29.893
29.879
29.842
29.829
29.806
29.620
29.573
29.547
26.330
26.308
22.862
14.256
f1 (ppm)

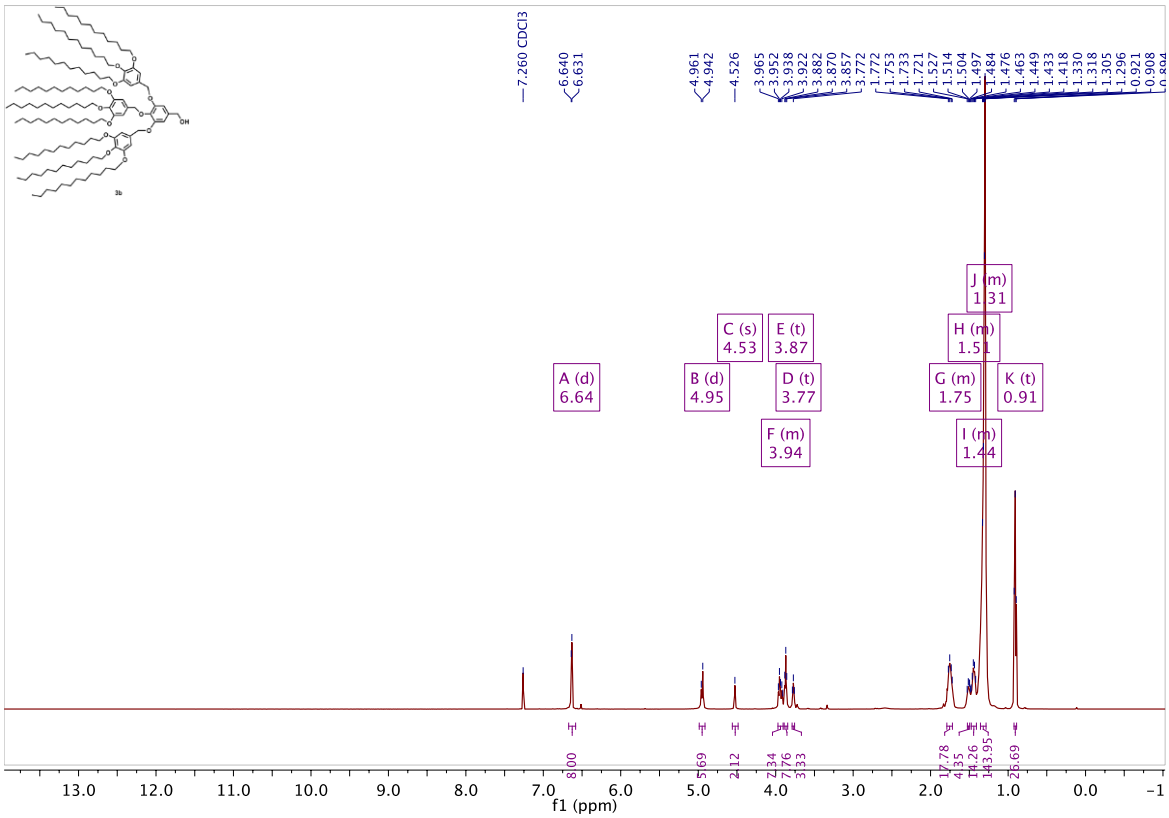
7.260 CDCl3
6.640
6.631
4.961
4.942
4.526
3.965
3.952
3.938
3.922
3.882
3.870
3.857
3.772
1.772
1.753
1.733
1.721
1.527
1.514
1.504
1.497
1.484
1.476
1.463
1.449
1.433
1.418
1.330
1.318
1.305
1.296
0.921
0.908
A (d) 6.64
B (d) 4.95
C (s) 4.53
D (t) 3.77
E (t) 3.87
F (m) 3.94
G (m) 1.75
H (m) 1.51
I (m) 1.44
J (m) 1.31
K (t) 0.91
8.00
5.69
2.12
7.34
7.76
3.33
17.78
4.35
14.26
43.95
26.69
f1 (ppm)

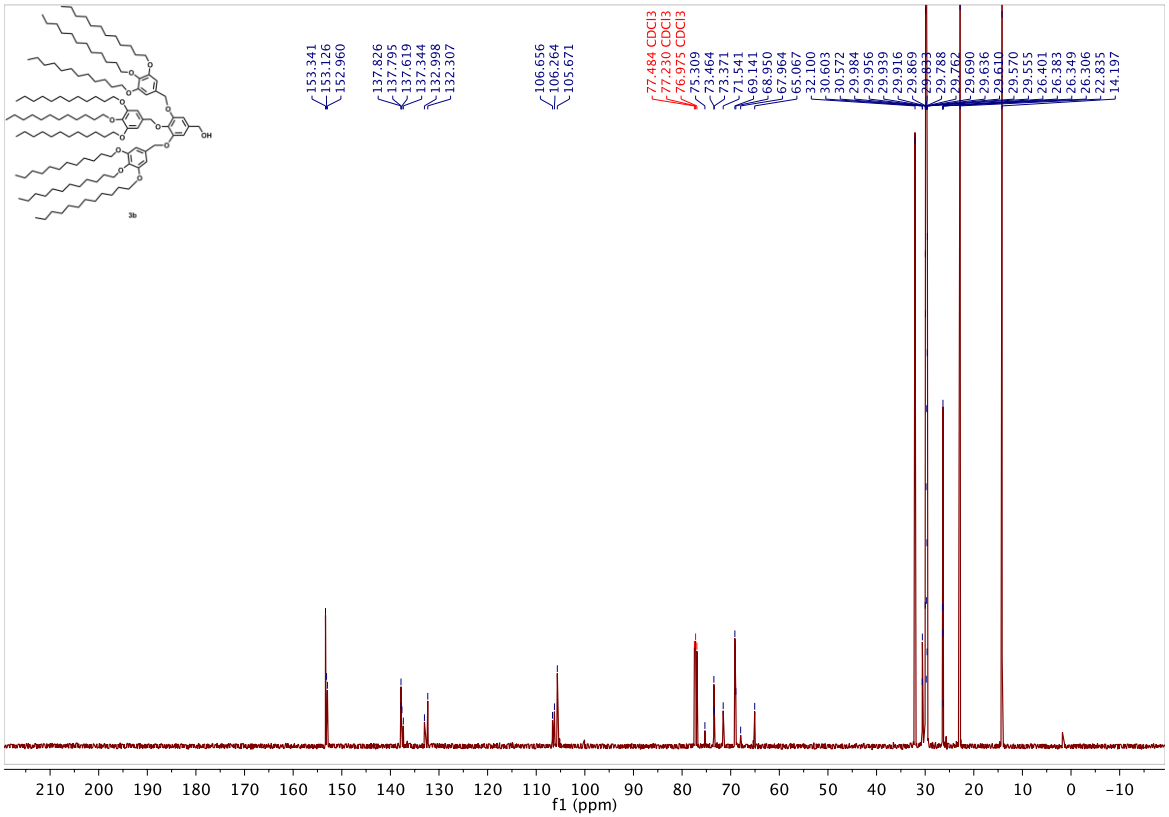
153.341
153.126
152.960
137.826
137.795
137.619
137.344
132.998
132.307
106.656
106.264
105.671
77.484 CDCl3
77.230 CDCl3
76.975 CDCl3
75.309
73.464
73.371
71.541
69.141
68.950
67.964
65.067
32.100
30.603
30.572
29.984
29.956
29.939
29.916
29.869
29.833
29.788
29.762
29.690
29.636
29.610
29.570
29.555
26.401
26.383
26.349
26.306
22.835
14.197
f1 (ppm)

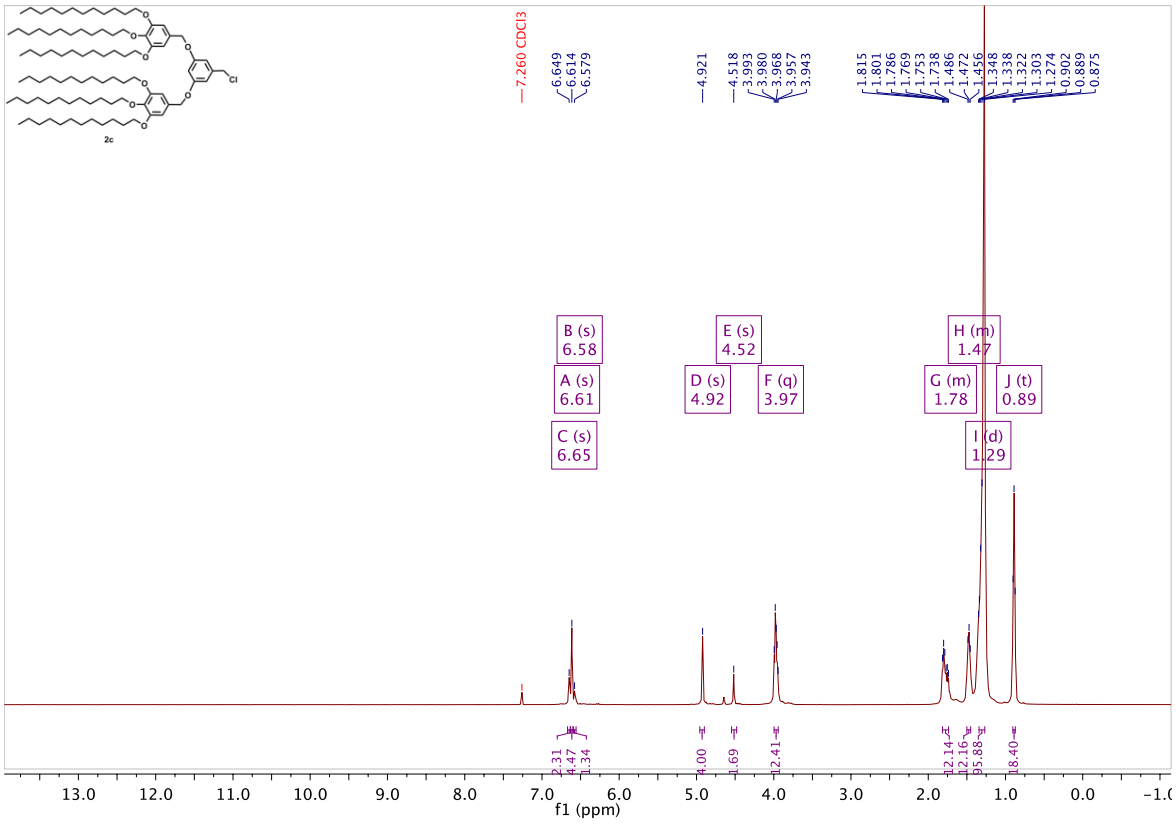
7.260 CDCl3
6.649
6.614
6.579
4.921
4.518
3.993
3.980
3.968
3.957
3.943
1.815
1.801
1.786
1.769
1.753
1.738
1.486
1.472
1.456
1.348
1.338
1.322
1.303
1.274
0.902
0.889
0.875
B (s) 6.58
A (s) 6.61
C (s) 6.65
E (s) 4.52
D (s) 4.92
F (q) 3.97
H (m) 1.47
G (m) 1.78
J (t) 0.89
I (d) 1.29
2.31
4.47
1.34
4.00
1.69
2.41
12.14
2.16
95.88
18.40
f1 (ppm)

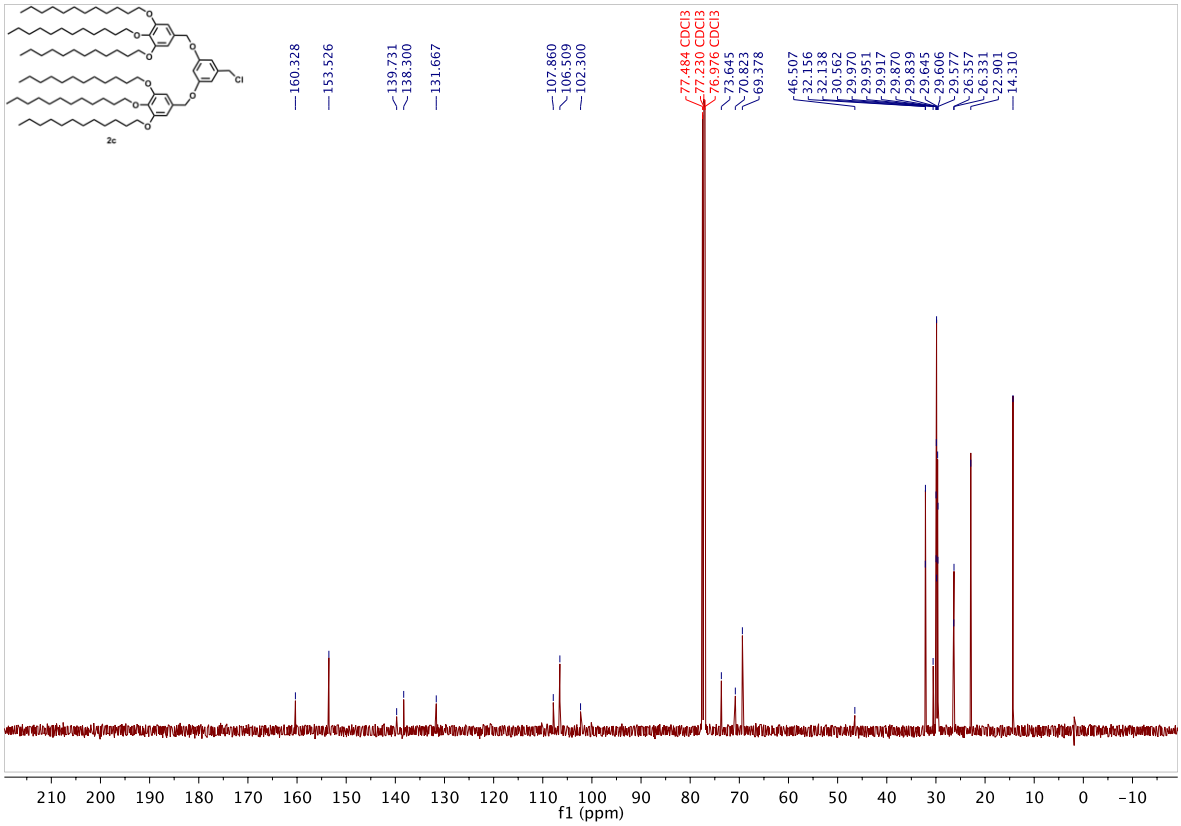
160.328
153.526
139.731
138.300
131.667
107.860
106.509
102.300
77.484 CDCl3
77.230 CDCl3
76.976 CDCl3
73.645
70.823
69.378
46.507
32.156
32.138
30.562
29.970
29.951
29.917
29.870
29.839
29.645
29.606
29.577
26.357
26.331
22.901
14.310
f1 (ppm)

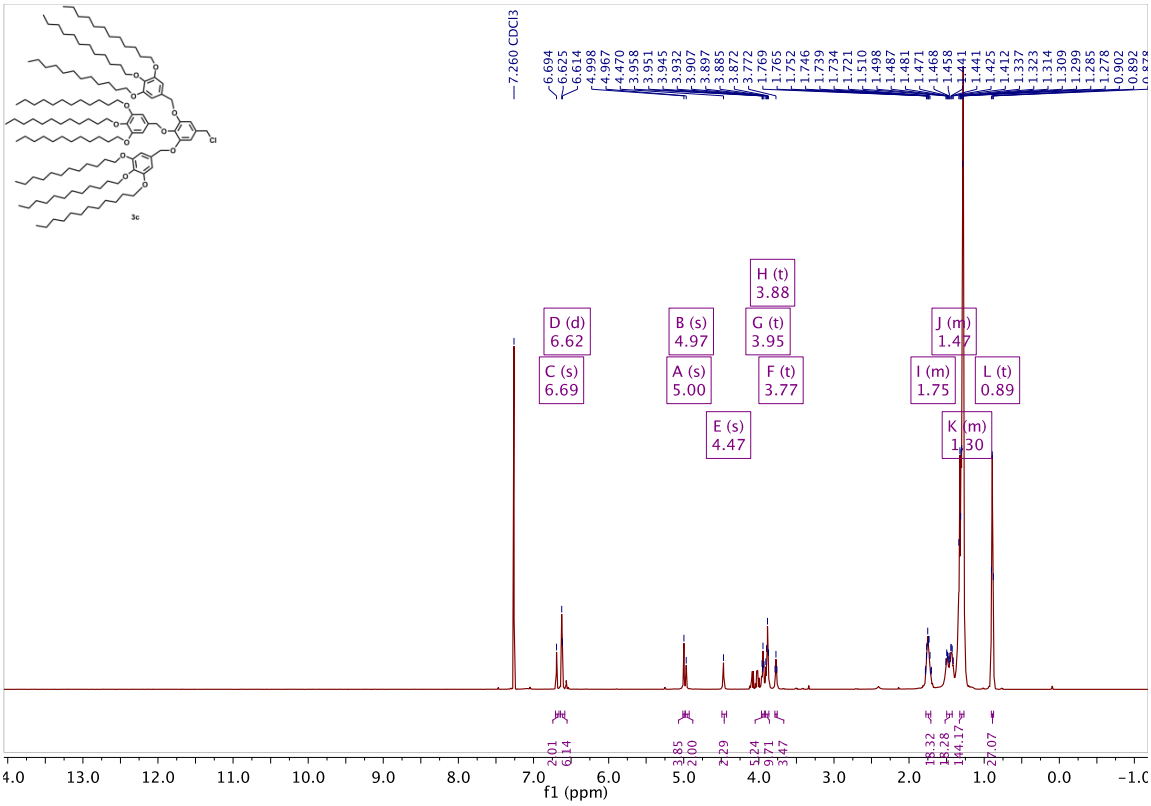
7.260 CDCl3
6.694
6.625
6.614
4.998
4.967
4.470
3.958
3.951
3.945
3.932
3.907
3.897
3.885
3.872
3.772
1.769
1.765
1.752
1.746
1.739
1.734
1.721
1.510
1.498
1.487
1.481
1.471
1.468
1.458
1.441
1.425
1.412
1.337
1.323
1.314
1.309
1.299
1.285
1.278
0.902
0.892
D (d) 6.62
C (s) 6.69
B (s) 4.97
A (s) 5.00
E (s) 4.47
H (t) 3.88
G (t) 3.95
F (t) 3.77
J (m) 1.47
I (m) 1.75
L (t) 0.89
K (m) 1.30
2.01
6.14
3.85
2.00
2.29
5.24
9.71
3.47
15.32
15.28
144.17
27.07
f1 (ppm)

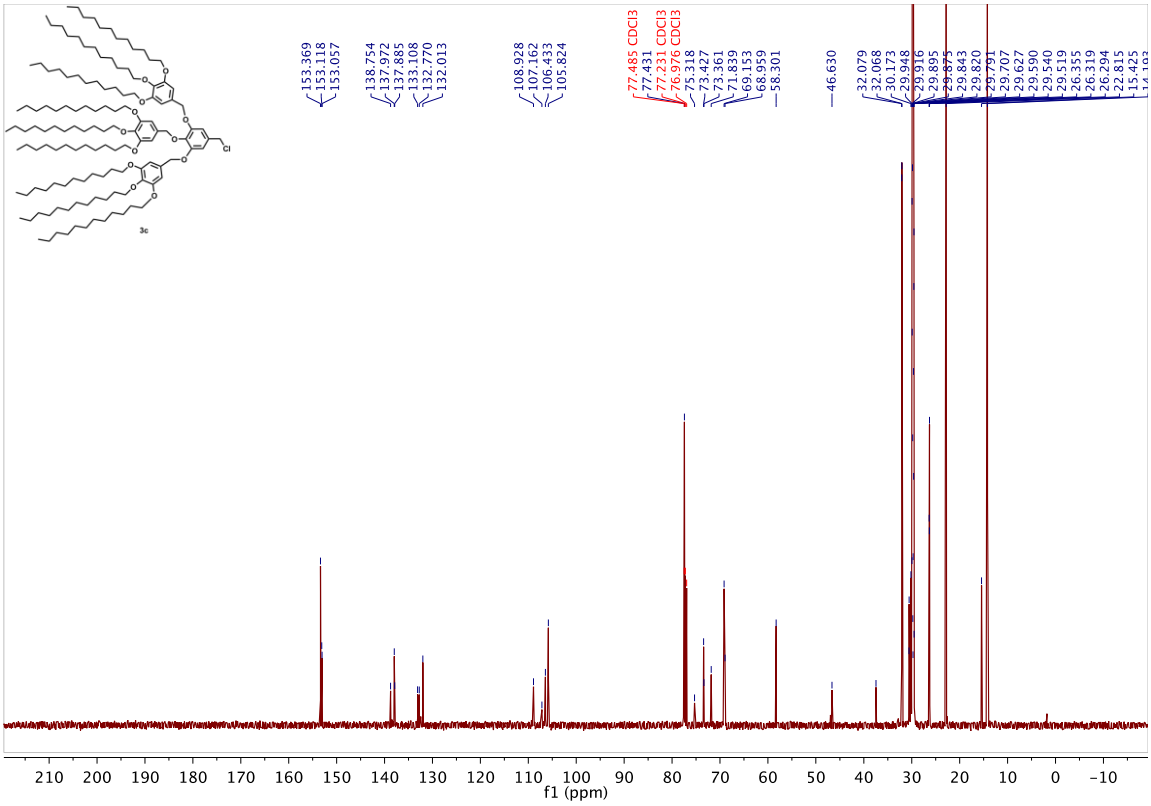
153.369
153.118
153.057
138.754
137.972
137.885
133.108
132.770
132.013
108.928
107.162
106.433
105.824
77.485 CDCl3
77.431
77.231 CDCl3
76.976 CDCl3
75.318
73.427
73.361
71.839
69.153
68.959
58.301
46.630
32.079
32.068
30.173
29.948
29.916
29.895
29.875
29.843
29.820
29.791
29.707
29.627
29.590
29.540
29.519
26.355
26.319
26.294
22.815
15.425
f1 (ppm)

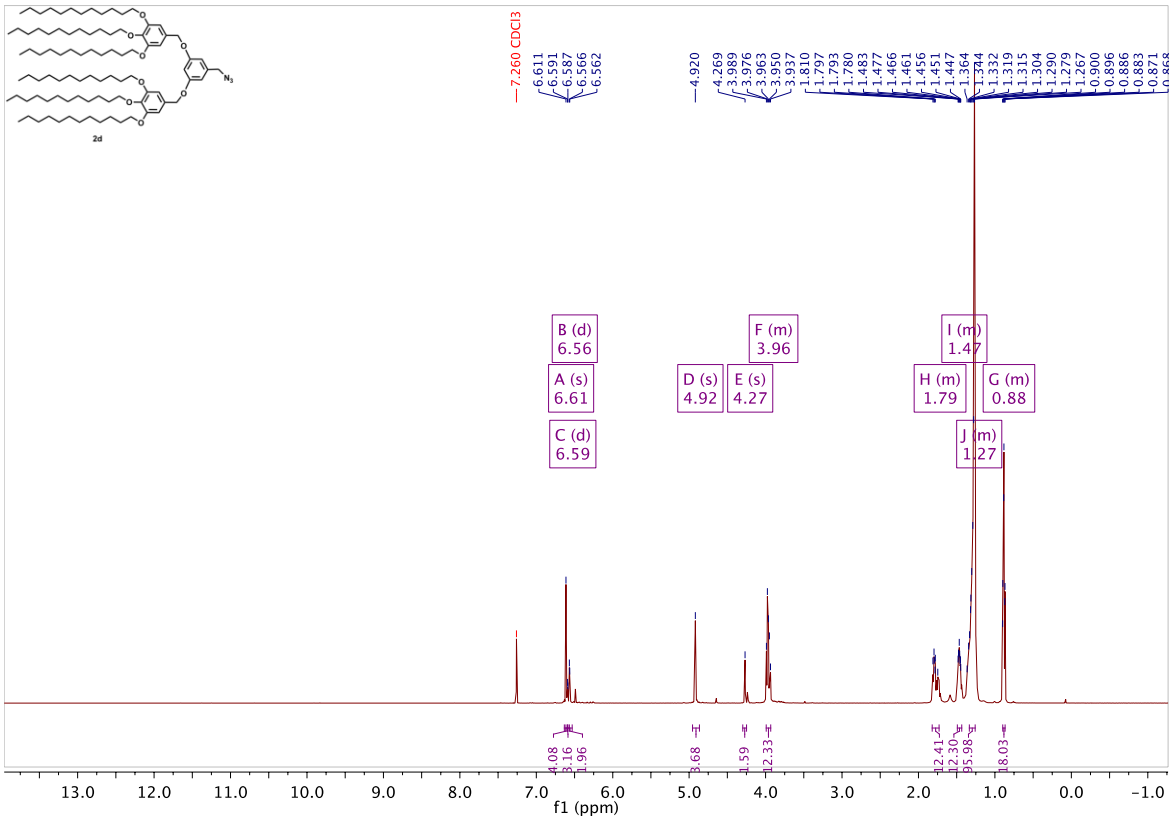
2d
7.260 CDCl3
6.611
6.591
6.587
6.566
6.562
4.920
4.269
3.989
3.976
3.963
3.950
3.937
1.810
1.797
1.793
1.780
1.483
1.477
1.466
1.461
1.456
1.451
1.447
1.364
1.334
1.332
1.319
1.315
1.304
1.290
1.279
1.267
0.900
0.896
0.886
0.883
0.871
B (d) 6.56
A (s) 6.61
C (d) 6.59
D (s) 4.92
E (s) 4.27
F (m) 3.96
I (m) 1.47
H (m) 1.79
G (m) 0.88
J (m) 1.27
4.08
3.16
1.96
3.68
1.59
2.33
12.41
12.30
15.98
18.03
13.0 12.0 11.0 10.0 9.0 8.0 7.0 6.0 5.0 4.0 3.0 2.0 1.0 0.0 -1.0
f1 (ppm)

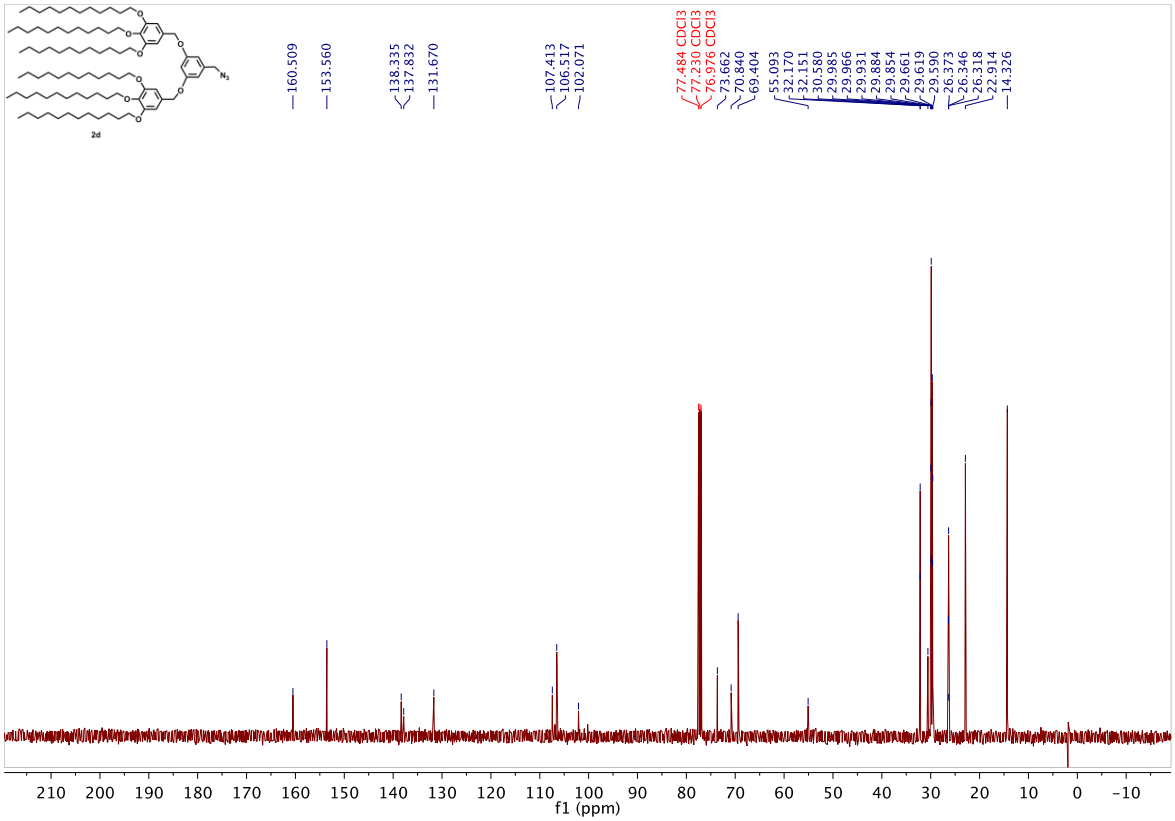
2d
160.509
153.560
138.335
137.832
131.670
107.413
106.517
102.071
77.484 CDCl3
77.230 CDCl3
76.976 CDCl3
73.662
70.840
69.404
55.093
32.170
32.151
30.580
29.985
29.966
29.931
29.884
29.854
29.661
29.619
29.590
26.373
26.346
26.318
22.914
14.326
210 200 190 180 170 160 150 140 130 120 110 100 90 80 70 60 50 40 30 20 10 0 -10
f1 (ppm)

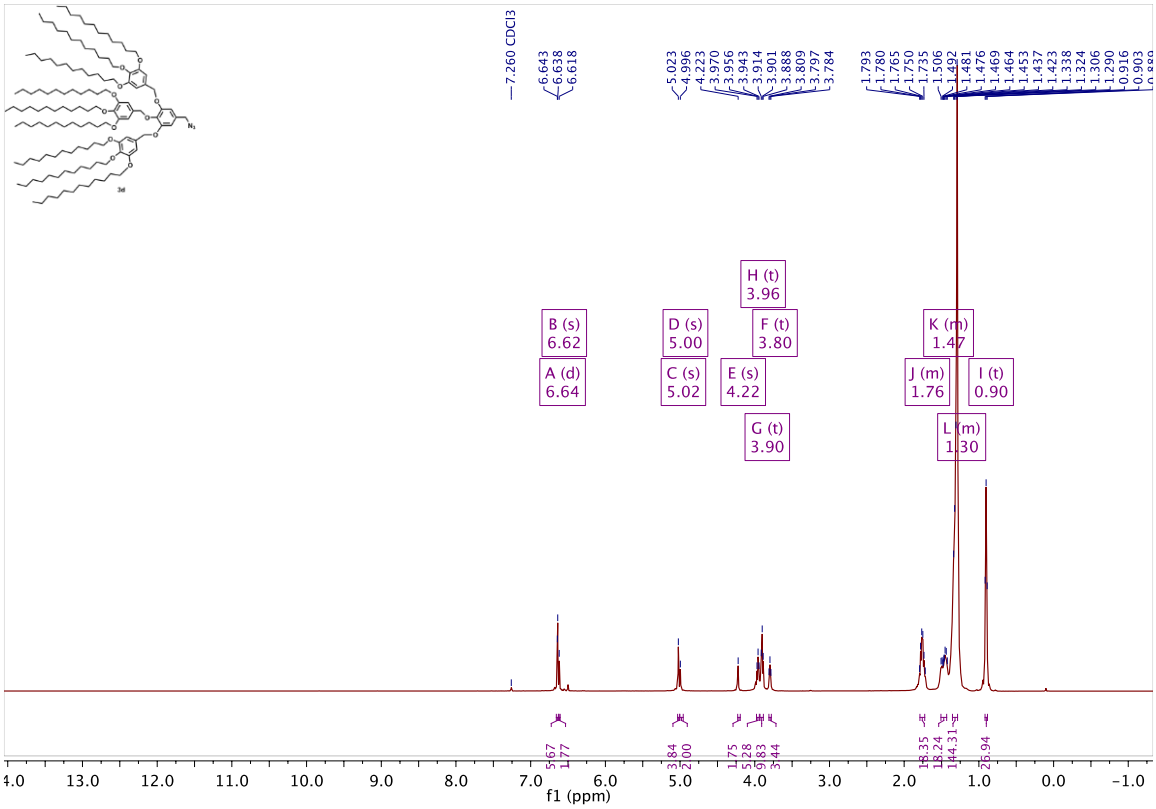
7.260 CDCl3
6.643
6.638
6.618
5.023
4.996
4.223
3.970
3.956
3.943
3.914
3.901
3.888
3.809
3.797
3.784
1.793
1.780
1.765
1.750
1.735
1.506
1.492
1.481
1.476
1.469
1.464
1.453
1.437
1.423
1.338
1.324
1.306
1.290
0.916
0.903
B (s) 6.62
A (d) 6.64
D (s) 5.00
C (s) 5.02
H (t) 3.96
F (t) 3.80
E (s) 4.22
G (t) 3.90
K (m) 1.47
J (m) 1.76
I (t) 0.90
L (m) 1.30
5.67
1.77
3.84
2.00
1.75
5.28
9.83
3.44
18.35
18.24
144.31
26.94
f1 (ppm)

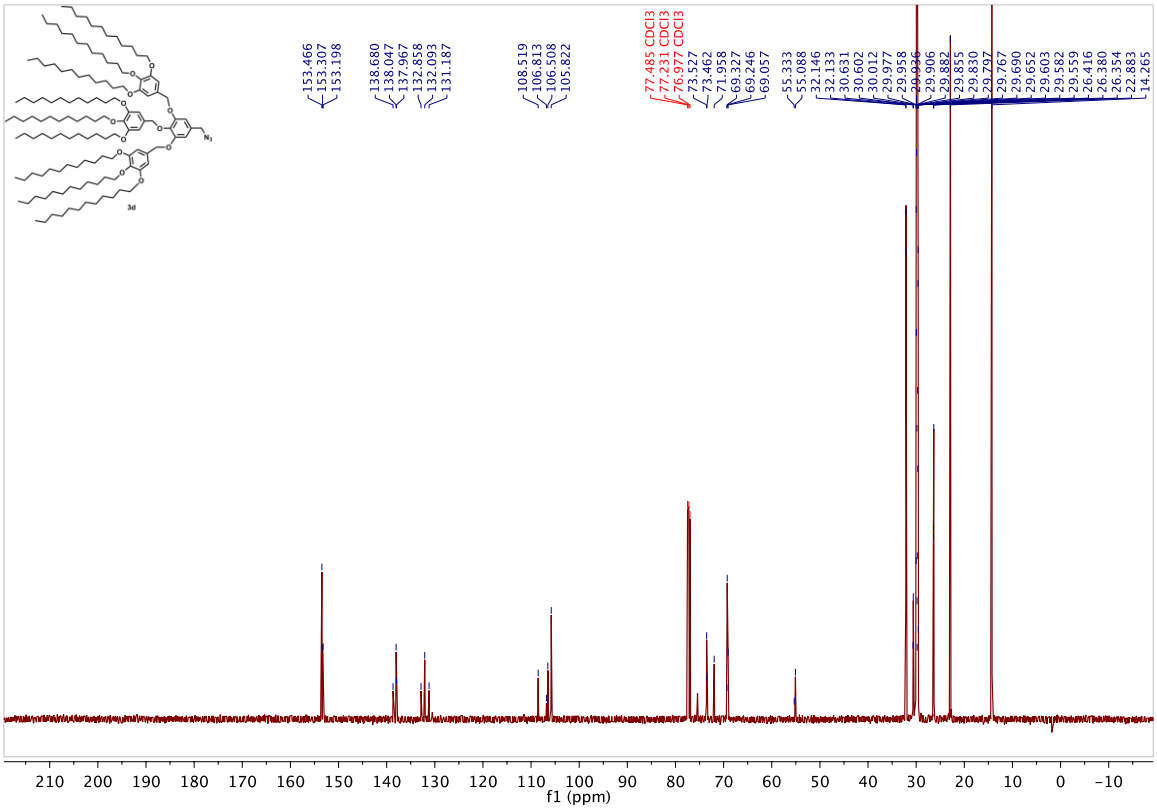
153.466
153.307
153.198
138.680
138.047
137.967
132.858
132.093
131.187
108.519
106.813
106.508
105.822
77.485 CDCl3
77.231 CDCl3
76.977 CDCl3
73.527
73.462
71.958
69.327
69.246
69.057
55.333
55.088
32.146
32.133
30.631
30.602
30.012
29.977
29.958
29.936
29.906
29.882
29.855
29.830
29.797
29.767
29.690
29.652
29.603
29.582
29.559
26.416
26.380
26.354
22.883
14.265
f1 (ppm)

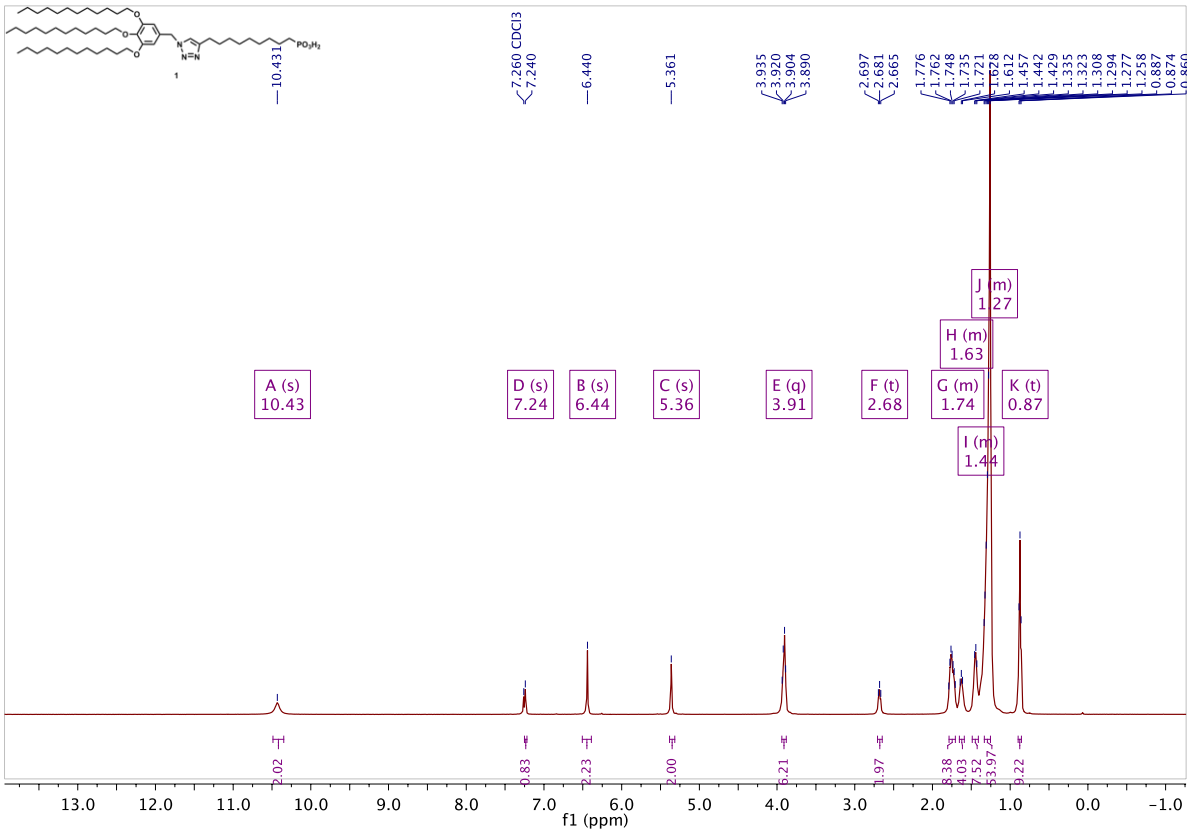
10.431
7.260 CDCl3
7.240
6.440
5.361
3.935
3.920
3.904
3.890
2.697
2.681
2.665
1.776
1.762
1.748
1.735
1.721
1.628
1.612
1.457
1.442
1.429
1.335
1.323
1.308
1.294
1.277
1.258
0.887
0.874
J (m) 1.27
H (m) 1.63
A (s) 10.43
D (s) 7.24
B (s) 6.44
C (s) 5.36
E (q) 3.91
F (t) 2.68
G (m) 1.74
K (t) 0.87
I (m) 1.44
2.02
0.83
2.23
2.00
6.21
1.97
8.38
4.03
7.52
53.97
9.22
13.0 12.0 11.0 10.0 9.0 8.0 7.0 6.0 5.0 4.0 3.0 2.0 1.0 0.0 −1.0
f1 (ppm)

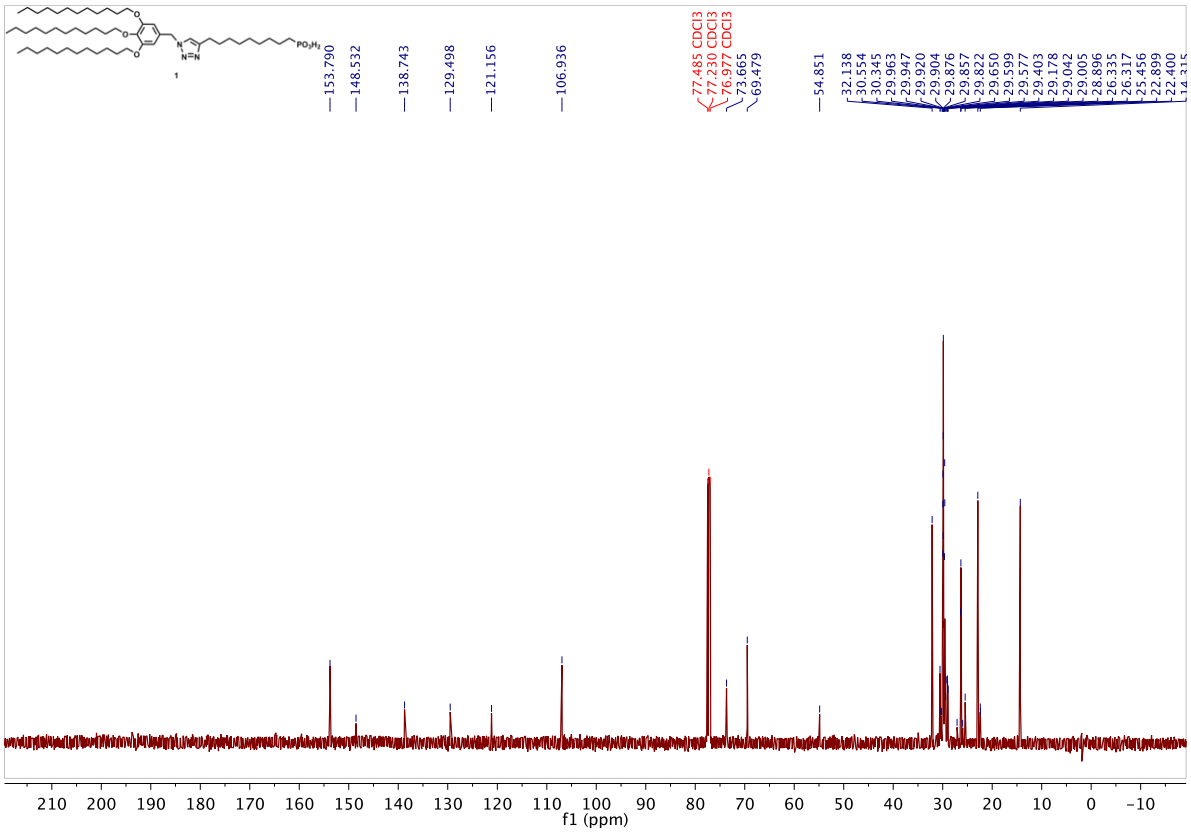
153.790
148.532
138.743
129.498
121.156
106.936
77.485 CDCl3
77.230 CDCl3
76.977 CDCl3
73.665
69.479
54.851
32.138
30.554
30.345
29.963
29.947
29.920
29.904
29.876
29.857
29.822
29.650
29.599
29.577
29.403
29.178
29.042
29.005
28.896
26.335
26.317
25.456
22.899
22.400
210 200 190 180 170 160 150 140 130 120 110 100 90 80 70 60 50 40 30 20 10 0 −10
f1 (ppm)

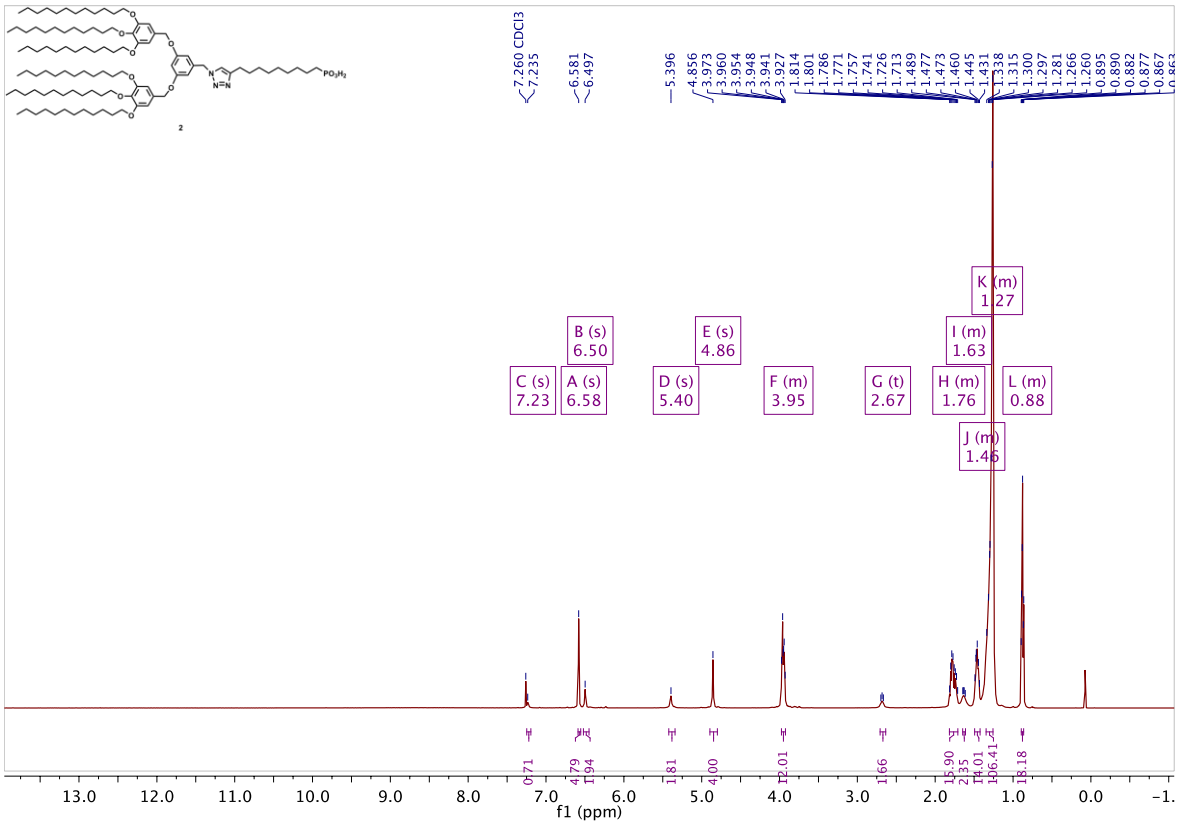
7.260 CDCl3
7.235
6.581
6.497
5.396
4.856
3.973
3.960
3.954
3.948
3.941
3.927
1.814
1.801
1.786
1.771
1.757
1.741
1.726
1.713
1.489
1.477
1.473
1.460
1.445
1.431
1.338
1.315
1.300
1.297
1.281
1.266
1.260
0.895
0.890
0.882
0.877
0.867
C (s) 7.23
A (s) 6.58
B (s) 6.50
D (s) 5.40
E (s) 4.86
F (m) 3.95
G (t) 2.67
H (m) 1.76
I (m) 1.63
J (m) 1.46
K (m) 1.27
L (m) 0.88
0.71
4.79
1.94
1.81
4.00
12.01
1.66
15.90
2.35
14.01
46.41
13.18
f1 (ppm)

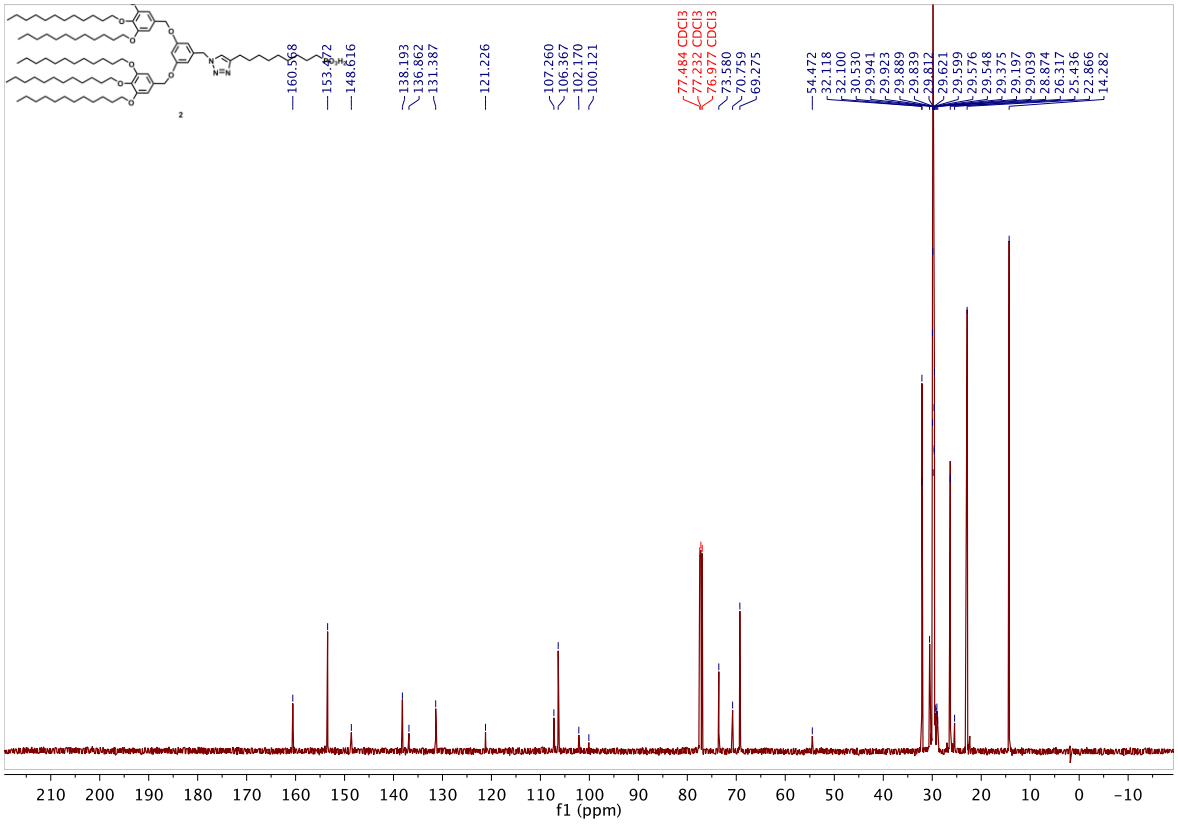
160.568
153.672
148.616
138.193
136.862
131.387
121.226
107.260
106.367
102.170
100.121
77.484 CDCl3
77.232 CDCl3
76.977 CDCl3
73.580
70.759
69.275
54.472
32.118
32.100
30.530
29.941
29.923
29.889
29.839
29.812
29.621
29.599
29.576
29.548
29.375
29.197
29.039
28.874
26.317
25.436
22.866
14.282
f1 (ppm)

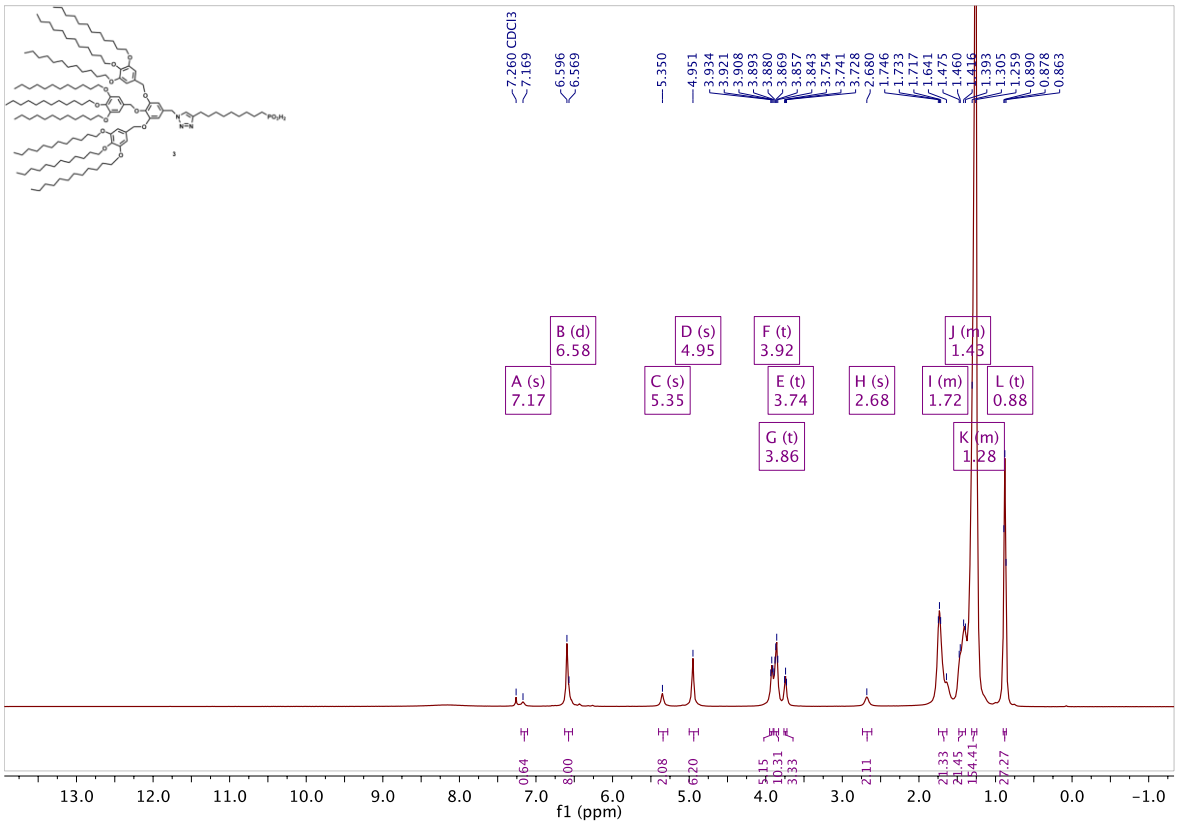
7.260 CDCl3
7.169
6.596
6.569
5.350
4.951
3.934
3.921
3.908
3.893
3.880
3.869
3.857
3.843
3.754
3.741
3.728
2.680
1.746
1.733
1.717
1.641
1.475
1.460
1.416
1.393
1.305
1.259
0.890
0.878
0.863
A (s) 7.17
B (d) 6.58
C (s) 5.35
D (s) 4.95
E (t) 3.74
F (t) 3.92
G (t) 3.86
H (s) 2.68
I (m) 1.72
J (m) 1.43
K (m) 1.28
L (t) 0.88
0.64
8.00
2.08
6.20
5.15
10.31
3.33
2.11
21.33
21.45
14.41
27.27
f1 (ppm)

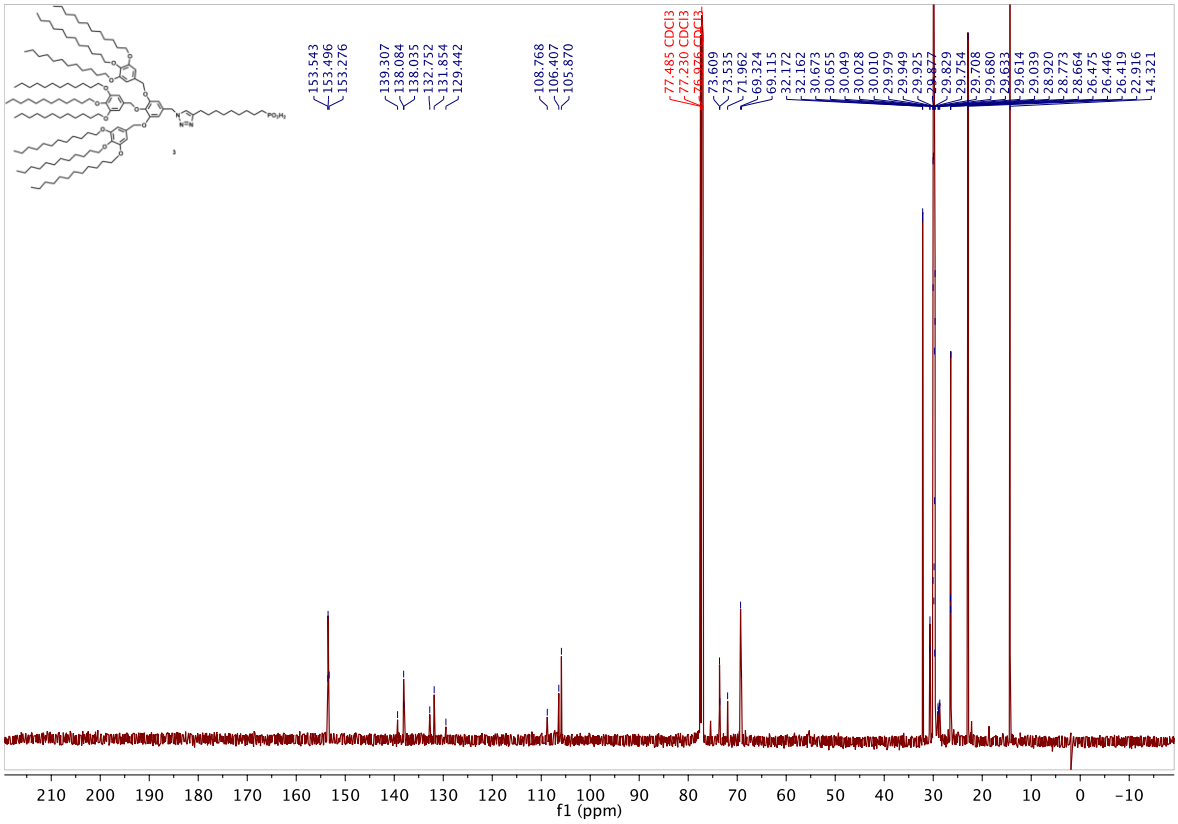
153.543
153.496
153.276
139.307
138.084
138.035
132.752
131.854
129.442
108.768
106.407
105.870
77.485 CDCl3
77.230 CDCl3
76.976 CDCl3
73.609
73.535
71.962
69.324
69.115
32.172
32.162
30.673
30.655
30.049
30.028
30.010
29.979
29.949
29.925
29.877
29.829
29.754
29.708
29.680
29.633
29.614
29.039
28.920
28.773
28.664
26.475
26.446
26.419
22.916
14.321
f1 (ppm)